JPET Fast Forward. Published on December 23, 2021 as DOI: 10.1124/jpet.121.000898
This article has not been copyedited and formatted. The final version may differ from this version.

TITLE The Andrographolide analogue 3A.1 synergizes with Taxane derivatives in aggressive metastatic prostate cancers by upregulation of Heat Shock proteins and downregulation of MAT2A-mediated cell migration and invasion

Taraswi Mitra Ghosh[1], Teeratas Kansom[1, 2], Suman Mazumder[1,4], Joshua Davis[1], Ahmed S. Alnaim[1], Shanese L. Jasper[1], Chu Zhang[1], Aedan Bird[1], Praneet Opanasopit[2], Amit K Mitra[1, 3,4], and Robert D. Arnold[1,3, *]

[1]Department of Drug Discovery & Development, Harrison School of Pharmacy, Auburn University, Auburn, AL, USA.

[2]Department of Pharmaceutical Technology, Faculty of Pharmacy, Silpakorn University, Thailand.

[3]University of Alabama at Birmingham O'Neal Comprehensive Cancer Center, Birmingham, AL, USA.

[4]Center for Pharmacogenomics and Single-Cell Omics Initiative, Auburn University, Auburn, AL, USA

***Corresponding Author:**

Robert D. Arnold, Ph.D.
Professor, Department of Drug Discovery & Development,
Auburn University, Harrison School of Pharmacy
Pharmaceutical Research Building
720 South Donahue Drive, Rm. 257
Auburn, AL 36849
Phone: (334) 844-8434
Email: rda0007@auburn.edu

RUNNING TITLE **Transcriptomics of 3A.1 and Taxane combination treatment in mCRPC**

Keywords: 3A.1, taxane, prostate, cancer, combination index, synergism, RNAseq, differential gene expression; DEGs, IPA, cell cycle; G1/S checkpoint, DNA damage, HSPs, MAT2A, MMPs.

Number of text pages - 39

Numbers of tables - 3 +1 Supplemental

Number of Figures - 5 +

Number of References - 64

Number of words in Abstract - 247 words

Number of words in Introduction - 600 words

Number of words in Discussion – 1458 words

Sections- Drug Discovery and translational Medicine

Metabolism, Transport and Pharmacogenomics

JPET Fast Forward. Published on December 23, 2021 as DOI: 10.1124/jpet.121.000898
This article has not been copyedited and formatted. The final version may differ from this version.

ABSTRACT

Conventional treatment with taxanes (docetaxel-DTX or cabazitaxel-CBZ) increases the survival rates of patients with aggressive metastatic castration-resistant prostate cancer (mCRPC), however, most patients acquire resistance to taxanes. The andrographolide analogue, 19-*tert*-butyldiphenylsilyl-8,7-epoxy andrographolide (3A.1), has shown anticancer activity against various cancers. In this study, we investigated the effect of 3A.1 alone and in combination with DTX/CBZ against mCRPC and their mechanism of action. Exposure to 3A.1 alone exhibited a dose- and time-dependent antitumor activity in mCRPC. Chou-Talalay's combination index (CI) values of all 3A.1+ TX combinations were less than 0.5, indicating synergism. Co-treatment of 3A.1 with TX reduced the required dose of DTX and CBZ ($p<0.05$). Caspase assay (apoptosis) results concurred with *in vitro* cytotoxicity data. RNAseq, followed by IPA analysis, identified that upregulation of heat-shock proteins (Hsp70, Hsp40, Hsp27, and Hsp90) and downregulation of MAT2A as the key player for 3A.1 response. Further, the top treatment-induced DEGs belong to DNA damage, cell migration, hypoxia, autophagy (MMP1, MMP9, HIF-1α, Bag-3, H2AX, HMOX1, PSRC1), and cancer progression pathways. Most importantly, top downregulated DEG MAT2A has earlier been shown to be involved in cell migration and invasion. Further, using *in silico* analysis on the TCGA database, we found that MAT2A and highly co-expressed ($r>0.7$) genes, TRA2B and SF1, were associated with worse Gleason score and nodal metastasis status in prostate adenocarcinoma patients (PRAD-TCGA). Immunoblotting, COMET, and migration assays corroborated these findings. These results suggest that 3A.1 may be useful in increasing the anticancer efficacy of taxanes to treat aggressive PCa.

JPET Fast Forward. Published on December 23, 2021 as DOI: 10.1124/jpet.121.000898
This article has not been copyedited and formatted. The final version may differ from this version.

SIGNIFICANCE STATEMENT

The andrographolide analogue, 19-*tert*-butyldiphenylsilyl-8,7-epoxy andrographolide (3A.1), has shown anticancer activity against metastatic Castration resistance and neuroendocrine variant prostate cancers (mCRPC/NEPC). Additionally, 3A.1 exhibited a synergistic anticancer effect in combination with standard therapy drug docetaxel and cabazitaxel in mCRPC/NEPC. Post-treatment gene expression studies revealed that heat shock proteins (Hsp70, Hsp40, Hsp27, and Hsp90) and MAT2A are the major players in the mechanism of 3A.1 action and drug response. Further, DNA damage, cell migration, hypoxia, and autophagy were the crucial pathways for the anticancer activity of 3A.1.

JPET Fast Forward. Published on December 23, 2021 as DOI: 10.1124/jpet.121.000898
This article has not been copyedited and formatted. The final version may differ from this version.

INTRODUCTION

Taxanes remain the only form of chemotherapy that improves survival in patients with metastatic castration-resistant prostate cancer (mCRPC). Docetaxel (DTX) and cabazitaxel (CBZ) are taxane derivatives that exert antitumor activity *via* microtubule destabilization when administrated as standard therapy for patients with (mCRPC)(Mukhtar *et al.*, 2016; Oudard *et al.*, 2017). Most patients acquire resistance to taxane drugs through alterations of androgen receptor (AR) signaling, tubulin structure, and multidrug-resistant phenotype(Corn *et al.*, 2019). In prostate cancer (PCa), taxanes have been reported to inhibit the ligand-induced AR nuclear translocation and activity of the androgen receptor along with downstream transcriptional activation of AR target genes such as prostate-specific antigen(Bai *et al.*, n.d.; Darshan *et al.*, 2011). Further, the development of DTX resistance involves overexpression of P-glycoprotein (P-gp; ATP-dependent drug efflux pump). The high substrate affinity of DTX for P-gp decreases intracellular drug concentrations and leads to ineffective treatment(Hwang, 2012; Quinn *et al.*, 2017). However, CBZ has poor substrate affinity for P-gp and showed improved antitumor activity in DTX-resistant CRPC patients(Duran *et al.*, 2015), but most patients given CBZ eventually develop chemo-resistance(Machioka *et al.*, 2018). The use of 2^{nd} generation antiandrogen therapy with enzalutamide, apalutamide, and/or abiraterone has shown activity in patients with mCRPC following DTX and CBZ; however, patients' diseases typically progress and ultimately develop drug resistance to these drugs (Scher *et al.*, 2012; Galletti *et al.*, 2017; Annala *et al.*, 2018). Further complicating treatment, approximately 25% of PCa patients develop aggressive treatment-resistant neuroendocrine variant prostate cancers (NEPC) (Yadav *et al.*, 2017).

Several anticancer compounds have been developed from natural sources, such as plants, to treat many types of cancers(Amin *et al.*, 2009; Demain and Vaishnav, 2011). Approved plant-derived chemotherapeutic agents include vincristine, vinblastine, etoposide, paclitaxel, docetaxel, topotecan, and irinotecan(Seca and Pinto, 2018). Andrographolide (AG) is the major bioactive component present in *Andrographis Paniculata*, a medicinal plant that has been used widely in complementary medicine in

China, India, Thailand, and Southeastern Asian countries with a broad range of pharmacological effects, including anti-inflammatory, antiviral, immunostimulatory, and anticancer activity(Varma *et al.*, 2011; Pawar *et al.*, 2016; Dai *et al.*, 2019). Previous studies have shown that AG possesses anti-prostatic activity by promoting DNA damage, cell cycle arrest, and apoptosis(Liu *et al.*, 2011; Wong *et al.*, 2011; Forestier-Román *et al.*, 2019). However, its poor bioavailability (2.67%; Andrographolide belongs to class III, as per BCS) and high dose requirements restrict its clinical potential(Ye *et al.*, 2011). The *in vivo* anti-tumor efficacy in PCa of AG was reported in cell line models as well as in tumor xenografts(Chun *et al.*, 2010; Forestier-Román *et al.*, 2019).

Structural modifications of andrographolide to improve its potency and efficacy as an anti-cancer drug have gained interest in recent times(Kansom *et al.*, 2018; Reabroi *et al.*, 2018). The semi-synthetic AG analogue, 3A.1 (19-*tert*—butyldiphenylsilyl-8,17-epoxy andrographolide) (**Figure 1A)**, developed in Dr. Saeeng's lab, exhibited greater anticancer activity than the parent compound (AG) and suppressed growth for several cancer cell lines, including cholangiocarcinoma (CCA) and colorectal cancer (CRC)(Nateewattana *et al.*, 2013, 2014; Kansom *et al.*, 2019). However, the effect of 3A.1 on prostate cancer is still unknown. Further, the mechanism of action (MOA) and key pathways governing 3A.1 drug action have not been comprehensively studied and fully elucidated.

The objective of this study was to determine the anticancer effects of 3A.1 as a single-agent and in combination with DTX or CBZ (**Figure 1A)** against AR- metastatic CRPC/NEPC taxane sensitive (PC-3, PC-3M, and DU145) and taxane resistant (DUTXR) AR- mCRPC human cell lines. The effects of taxanes administered as single drugs were compared with the effects of 3A.1 administered alone or in combination with taxanes (DTX/CBZ) treatment on cell growth, cytotoxicity, cellular migration, and apoptosis. Next-generation RNA sequencing (RNAseq)-based gene expression studies were performed to gain mechanistic insights into the activity of 3A.1 after single-agent and combination (DTX/CBZ) administration. Treatment-specific differential gene signatures (DEGs) were identified, and protein expression was confirmed by immunoblot analysis. Overall, these data suggest that 3A.1 acts synergistically with DTX or CBZ to treat

JPET Fast Forward. Published on December 23, 2021 as DOI: 10.1124/jpet.121.000898
This article has not been copyedited and formatted. The final version may differ from this version.

taxane-sensitive and resistant mCRPCs/NEPC cells. Future preclinical translational studies are needed to assess *in vivo* activity of 3A.1 and further delineate its MOA.

JPET Fast Forward. Published on December 23, 2021 as DOI: 10.1124/jpet.121.000898
This article has not been copyedited and formatted. The final version may differ from this version.

MATERIALS AND METHODS

Chemicals and Reagents

Fetal bovine serum (FBS), trypsin (0.25 % w/v), F-12K Nutrient Mixture (Kaighn's Mod.), Eagle's Minimum Essential Medium (EMEM), and RPMI-1640 medium were purchased from Hyclone (Thermo Fisher Scientific Inc. Rockford, IL). Dimethyl sulfoxide (DMSO), sulforhodamine B (SRB), TRIS buffer, acetic acid, and Pierce ECL western blotting substrate for chemiluminescence were obtained from Bio-RAD (Hercules CA, USA). 3-(4,5-dimethylthiazol-2-yl)-2,5-diphenyltetrazolium bromide (MTT), propidium iodide (PI), phosphate-buffered saline (PBS), and RNAse A were purchased from Sigma-Aldrich Inc (St. Louis, MO). Mouse anti-human antibodies (Hsp90, Hsp70, Hsp40, Hsp27, MMP-9, MMP-1, HIF1α, MAT2A, H2AX, and Beta-actin) were purchased from Abcam (Cambridge, MA). Goat anti-mouse IgG (H=L) secondary antibody was purchased from ThermoFisher Scientific (Waltham, MA). 3A.1, as an andrographolide analogue with 95% purity, was kindly gifted from Dr. Rungnapha Saeeng from Burapha University Thailand. DTX and CBZ with 98% purity were purchased from Advanced ChemBlocks Inc. (Burlingame, CA, USA). Caspase-Glo® 3/7 assay kit was obtained from Promega (Madison, WI, USA).

Cell Lines

Human PCa cell lines PC-3, PC-3M and DU145 (representing metastatic castration resistance-mCRPC with nonendocrine differentiation, NEPC (Yuan *et al.*, 2007; Sun *et al.*, 2009) were obtained from American Type Culture Collection (ATCC, Rockville, MD, USA). DUTXR (DU145 taxanes resistance) was generated and gifted by our collaborator Dr. Amit Kumar Mitra, from Auburn University. All cell lines were authenticated at their source and tested at regular intervals for mycoplasma; all cell lines were negative for mycoplasma, showed typical morphology, and they showed consistent patterns of potency (IC_{50}) using standard drugs and established cytotoxicity assays. Further, all cell lines were authenticated by STR analysis performed at the AU Center for Pharmacogenomics and Single-Cell Omics (AU PharmGx). PC-3 and PC3M cells were maintained in 10% (v/v) FBS supplemented F-12K, DU145 in EMEM, and DUTXR cells were maintained in RPMI-1640 medium supplemented with 0.02 nM paclitaxel; all cells were kept at

JPET Fast Forward. Published on December 23, 2021 as DOI: 10.1124/jpet.121.000898
This article has not been copyedited and formatted. The final version may differ from this version.

37ºC, 21% O_2 and 5% CO_2 in a humidified cell culture chamber (Heracell Vios 160i CO; Thermo Scientific). Cell lines were routinely sub-cultured when they reached approximately 80-90% confluence.

Single-agent and Combination treatment protocols

PCa (mCRPC) cell lines were seeded at 4×10^3 cells/well in 96 well plates with appropriate media with 10% (v/v) FBS supplemented[35]. Plates were incubated for 24 h prior to media change and replacement with serum-supplemented media containing DTX (0.2–3,600 nM), CBZ (0.2–3,600 nM) and 3A.1 (0.625-80 μM) for single-drug treatments. Whereas, for co-treatment, two pairs of drugs, DTX plus 3A.1 and CBZ plus 3A.1 at a constant molar ratio of a single dose (1:200), were added. Plates were then incubated at the same conditions for an additional 48 h. All experiments were performed in triplicates (n = 3) with six replicates well for each concentration of each drug as single agent and combinations. Cell growth and cytotoxicity were assessed at each time point.

Assessment of cell growth and cytotoxicity

The effect of DTX, CBZ, and 3A.1 treatment on PCa (mCRPC) cell growth and cytotoxicity were assessed by measuring mitochondrial enzyme activity (MTT) and total protein (SRB). Briefly, MTT and SRB staining was performed at 48 h after initial drug exposure(Aljuffali *et al.*, 2011). Absorbance was measured at 490 nm using a Synergy HT Multi-Mode Microplate Reader. The effect of drug exposure was determined by constructing cytotoxicity (growth) curves (n=6 wells/group); percent change relative to untreated controls was calculated at each drug concentration. Half-maximal inhibitory drug concentration (IC_{50}) values were estimated by nonlinear regression using a sigmoidal dose-response equation (variable slope - three parameters).

Assessment of drug interaction (combination study)

To evaluate the pharmacological interactions, the percentage (%) of cells affected (fraction affected - Fa) by DTX or CBZ and 3A.1 treatment in combination were analyzed by CompuSyn version 1.0 software (ComboSyn Inc., Paramas, NJ, USA). Combination index (CI) values were calculated according to Chou

JPET Fast Forward. Published on December 23, 2021 as DOI: 10.1124/jpet.121.000898
This article has not been copyedited and formatted. The final version may differ from this version.

Talalay's method(Chou and Talalay, 1984). The CI values <1, =1, and >1 refer to synergistic, additive, and antagonistic effects of the drugs treated in combination, respectively. Dose reduction index (DRI) was calculated for each drug combination of all cell lines, where DRI > 1 indicates that reduced dose (RD) requirement of a specific drug in drug combination compared with the dose of the same drug as single-drug treatment.

Apoptosis assay (caspase3/7)

Caspase-3/7 activation was measured by using the Caspase-Glo 3/7 assay (Promega Corporation) according to the manufacturer's protocol. Briefly, a total of 2×10^4 cells/well were seeded into 96-well white plates (triplicates). Each cell line was exposed for 24 h to seven different treatments; as follows, 1) DTX at estimated 48 h MTT-IC_{50}, 2) CBZ at estimated 48 h MTT-IC_{50}, 3) 3A.1 at estimated 48 h MTT-IC_{50}, 4) DTX 48 h MTT-IC_{50} + 3A.1 48 h MTT-$IC_{50,}$ 5) CBZ 48 h MTT-IC_{50} + 3A.1 48 h MTT-IC_{50} 6) DTX-RD + 3A.1-RD and 7) CBZ-RD + 3A.1-RD. Caspase-Glo 3/7 reagent was added to each well, agitated on a plate shaker, and plates were returned to the same conditions for 2 h, and luminescence was measured using Synergy 3 plate reader (BioTek Instruments). Apoptosis in each treatment group was normalized with the control group (no drug treatment or baseline caspase 3/7 assay luminescence) for each cell line.

Assessment of cellular morphology:

Cell morphology was assessed using phase-contrast microscopy. All cell lines were seeded in 6-well plates (4×10^3 cells/well) and exposed for 48 h to different treatments as described above in the apoptosis assay. Three areas with approximately equal cell densities were identified in each well, and images were captured with EVOS FL digital cell imaging system (Thermo Fisher Scientific, Inc.). Images were recorded in bright field and phase contrast modes at 20× and 40× magnifications. A blinded investigator and a blinded observer were captured and analyzed images using ImageJ software (https://imagej.net/ImageJ).

Migration Assay

JPET Fast Forward. Published on December 23, 2021 as DOI: 10.1124/jpet.121.000898
This article has not been copyedited and formatted. The final version may differ from this version.

Cellular migration was determined by creating a "scratch" in a cell monolayer followed by capturing the images at the beginning and regular interval (0, 24, and 48 h for all treatments) during cell migration to close the scratch and comparing the images to quantify the migration rate of the cells. Briefly, mCRPC cell lines (PC3 and DUTXR) were plated in 6-well plates at 1×10^5 cells/well and incubated for 48 h to 90% confluency. The monolayer was scratched with a SPLScar Scratcher 6 well Tip Width 0.50 mm sterile at the center of the well. The appropriate culture medium, supplemented with 10% FBS and containing the vehicle (0.05 % DMSO) was added to the cells in the control wells, and micrographs were obtained at 0, 24, and 48 h. DTX, CBZ, and 3A.1 as single-agent or TX+3A.1 combination doses were applied to the cells in the respective wells, and micrographs of the wound areas were obtained at 0 and 48 h using an EVOS FL digital cell imaging system (Thermo Fisher Scientific, Inc.) and BioTek Cytation5. The area of the initial wound (at 0 h) and the "gap area" were measured at 48 h with ImageJ software by a blinded investigator and a blinded observer.

Next-generation RNA sequencing (RNAseq)

PCa cells were plated at a density of 4×10^3 cells/ml, and after 24 h incubation for single-agent treatment, the lowest estimated MTT-IC_{50} for each drug was added to each cell line, whereas for combination estimated lowest MTT-IC_{50} for both drugs were added. Cells were collected 24 h post-treatment as baseline (0 nM/untreated) and post-treatment (treated). High-quality RNA was extracted from untreated and treated PCa cells using QIAshredder and RNeasy kit (Qiagen). RNA concentration and integrity were assessed using the Nanodrop-8000 and an Agilent 2100 Bioanalyzer and stored at −80 °C. RNA integrity number/RIN threshold of eight was used for RNA-seq analysis. RNA-seq libraries were constructed using Illumina TruSeq RNA Sample Preparation kit v2. Libraries were then size selected to generate inserts of ~200 bp. RNA sequencing was performed on llumina's NovaSeq next-generation high-throughput sequencing system using 150 bp paired-end protocol with a depth of >20 million reads per sample. The average quality scores were above Q30 for all libraries in both R1 and R2.

RNA-seq data processing

JPET Fast Forward. Published on December 23, 2021 as DOI: 10.1124/jpet.121.000898
This article has not been copyedited and formatted. The final version may differ from this version.

RNA-seq data were normalized, and fragments per kilobase million values were used in further analysis using Partek Flow data analysis software. Quality control (QC) check on the RNA-seq raw reads was performed using the FastQC tool, followed by read trimming to remove base positions with a low median (or bottom quartile) score. STAR Aligner tool mapped processed RNA-seq reads to the hg19 human genome build. Gene expression analysis following 3A.1 single-agent treated for the anti-apoptotic genes (BCL2L1, CAPN2, TNFRSF1A, CAPN1, IRAK1, PRKACA, AKT1, NFKBIA, PIK3R2) and the pro-apoptotic genes TNFRSF10B, DFFA, RELA, TRADD, and MYD88 was determined.

Bioinformatics analysis

Gene expression data were filtered using the following criteria: genes with mean FPKM < 1 were removed. GEP data were analyzed further using a combination of R and Partek Flow to perform differential expression testing to identify GEP signatures of drug response. Mean fold-change >|1| and $p<0.05$ were considered thresholds for reporting significant differential gene expression. Differentially expressed (DEG) gene analysis was performed between two groups of gene expression data sets (e.g., treated vs. untreated). Heatmaps were generated using unsupervised hierarchical clustering (HC) analysis based on the DEG genes. Owing to the small sample size, Limma, an empirical Bayesian method, was used to detect DEGs, obtain p values, and further provided a False discovery rate (FDR) based on the p-value using the Benjamini–Hochberg procedure to detect the DEGs (Ritchie *et al.*, 2015). The advantage of Limma compared with a traditional t-test is that it provides a moderated t-test statistic by shrinking the variance statistics, therefore, improves the statistical power.

Statistical analysis

All statistical analyses were performed using R for statistical computing and graphics, version 3.4.2, and GraphPad Prism version 7.0. We used parametric methods to analyze differences between two groups of cells. If the assumption appears violated, appropriate non-parametric procedures were used. All tests were two-sided, and differences with a $p<0.05$ were considered statistically significant.

JPET Fast Forward. Published on December 23, 2021 as DOI: 10.1124/jpet.121.000898
This article has not been copyedited and formatted. The final version may differ from this version.

Ingenuity pathway analysis (IPA)

IPA (Ingenuity® Pathway Analysis, QIAGEN) was used to identify the most significantly affected i) molecular pathways predicted to be activated or inhibited ii) upstream regulator molecule like miRNA, transcription factors iii) downstream effects and biological processes that are increased or decreased iv) predicted causal networks, relationships, mechanisms and functions relevant to changes observed in our dataset (Krämer *et al.*, 2014).

Assessment of cell cycle

Cell cycle was assessed at different treatments as described above (Apoptosis assay (caspase3/7) for 48 h for all cell lines. Briefly, cells were prepared for cell cycle analysis by staining with PI (50 µg/ml) in sample buffer [PBS + 1% (w/v) glucose], containing RNAse A (100 units/mL) for 30 min at room temperature and analyzed by flow cytometry using a Becton Dickinson FACS Calibur flow cytometer (BD Biosciences, San Jose, CA). Cell cycle data were analyzed using CytExpert (Beckman Coulter Inc, Indianapolis, IN). Data are presented as the mean ± SEM of three separate experiments (n = 5/study).

Assessment of DNA damage

DNA damage due to 3A.1 treatment was assessed using COMET Assay. Briefly, mCRPC cell lines were plated in 6-well plates at 1×10^5 cells/well and incubated at 37°C in an atmosphere of 5% CO_2 for 48 h to a 90% confluency. After 24 h incubation cell lines were treated with the corresponding IC_{50} of 3A.1 for each cell line. Trevigen's Comet Assay or single cell gel electrophoresis assay was performed for all cell lines according to the manufacturer's protocol.

Immunoblotting

PCa cells were seeded and exposed to drugs at the corresponding IC_{50} of each treatment protocol. Post-treatment cells were lysed in cell lysis buffer (Thermo Scientific RIPA Lysis and Extraction Buffer). Quantification of proteins was performed using Bradford assay and a calibration curve of protein content was created from the BSA protein standard kit (Bio-Rad Laboratories Inc., CA, USA). An equal amount of

protein was loaded onto 4-15% Criterion TGX Stain-Free Precast Gels. Proteins were separated under reducing conditions and then transferred to a PVDF membrane using a Trans-Blot Turbo Mini transfer pack from BioRad. Nonspecific binding was limited by incubating the membrane in blocking buffer (2.5% (w/v) casein, pH 7.6, 150 mM NaCl, 10 mM TRIS-HCl, and 0.02% sodium azide). Membranes were incubated with primary antibodies for targeted gene/protein (1:1000) overnight and then with the appropriate secondary antibody (1:10,000) for 1.5 h at room temperature. Immunoreactivity was detected using Pierce ECL Western Blotting substrate (Bio-Rad, CA). Images were captured and quantified using a Gel Doc™ EZ Gel Documentation System and ImageLab Software (Bio-RAD, CA). Densitometry analysis was performed using image analysis software ImageJ.

In silico validation using Cancer Genome Atlas (TCGA) database

Gene expression data on PCa patient cohort was obtained from the TCGA data portal (The Genomic Data Commons (GDCs) server). These include mRNA expression data on 717 PCa patients (500 prostate adenocarcinoma) and (217 cases from the Foundation Medicine Adult Cancer Clinical Dataset). We used UALCAN, an interactive web portal to perform an in-depth analysis of TCGA transcriptome data on the gene expression signatures obtained from our RNAseq studies as well as candidate pathway genes(Chandrashekar *et al.*, 2017).

JPET Fast Forward. Published on December 23, 2021 as DOI: 10.1124/jpet.121.000898
This article has not been copyedited and formatted. The final version may differ from this version.

RESULTS

In vitro growth assays (single agent)

The effect of single-agent administration, DTX, CBZ, and 3A.1, on PCa cells, was assessed by measurement of MTT and SRB absorbance after 48 h exposure (**Figure 1 B and C**). Single drug exposure resulted in significant ($p \leq 0.05$) time-dependent decreases in MTT and SRB in IC_{50} after 48 h (**Table 1**). IC_{50} and AUC values of DTX, CBZ, and 3A.1 single-agent treatment in PC3, PC3M, DU145, and DUTXR cell lines exhibited inter-individual variation in response. (**Figure 1B and C**., **Table 1**). Similar results were observed after 48 h of treatment as measured by the SRB assay.

3A.1 shows synergy with Taxanes (combination study)

The effect of DTX + 3A.1 and CBZ + 3A.1 combination treatment on PC3, PC3M, DU145, and DUTXR cell lines was assessed after 48 h treatment by MTT and SRB. Drug combinations exhibited synergistic effect (CI< 1) and predicted Dose Reduction (DRI>1) for DTX, CBZ, and 3A.1 observed at IC_{50}, $IC_{75,}$ and IC_{90} (**Figure 2A and Supplementary Figure 1**). The CI values ranged between 0.25-0.79, 0.35-0.76, and 0.45-0.9 at IC_{50}, $IC_{75,}$ and $IC_{90,}$ respectively (**Table 2**) for 3A.1 and taxane combination treatment. Additionally, DRI indicated dose reduction (RD) of both the drugs (taxanes; 3A.1 and DTX or CBZ) in combination, ranging from 2-15, 1.5-255, and 1-1000 at IC_{50}, $IC_{75,}$ and $IC_{90,}$ respectively (**Table 2**). This indicates a lower requirement of the drugs in combination to achieve the same cell killing.

Apoptosis (caspase-3/7 activation) assays

Schedule-dependent effects on apoptosis were determined by measuring the activity of caspase-3/7 following treatment (DTX, CBZ, and 3A.1 at their estimated IC_{50} for single-agent vs. combinations) (**Figure 2B**.). Combination treatment with DTX+3A.1 (PC3 6.6-, PC3M 7.0-, DU145 3.6- and DUTXR 3.5-fold) and CBZ+3A.1(PC3 5.7-, PC3M 6.8-, DU145 3.4-, and DUTXR 3.4-fold) induced apoptosis in every cell line compared to cells with single-agent treatment (**Figure 2B**). Consistent with the results

JPET Fast Forward. Published on December 23, 2021 as DOI: 10.1124/jpet.121.000898
This article has not been copyedited and formatted. The final version may differ from this version.

from the growth assays, apoptosis assay showed combination treatment to be a more effective treatment schedule as compared with single-agent therapy. Concurrently, gene expression analysis of treated vs. 3A.1 single-agent treated PCa samples showed downregulation of anti-apoptotic genes (BCL2L1, CAPN2, TNFRSF1A, CAPN1, IRAK1, PRKACA, AKT1, NFKBIA, PIK3R2) (**Figure 2C**) and upregulation of the pro-apoptotic genes TNFRSF10B, DFFA, RELA, TRADD, and MYD88 (data not shown). This provided additional support that 3A.1 treatment induces apoptosis *in vitro*. Gene set involved in the major pathways of cellular apoptosis were downloaded from the KEGG (Kyoto Encyclopedia of Genes and Genomes; KEGG_APOPTOSIS) database.

Cell Morphology study

Cell morphology studies, as shown in **Figure 2D**, confirmed the differences in the IC_{50} values (MTT and SRB staining) as well as apoptosis assays. PCa cells exposed to combination treatment regimens showed greater percent decreases in cellular density than single-agent treatments. For 3A.1+DTX combination (RD), the fold change decreased were PC3 3.6-, PC3M 3.9-, DU145 4.6-, and DUTXR 3.2-fold for 3A.1+DTX, while for 3A.1+CBZ, these were: PC3 4.4-, PC3M 4.2-, DU145 4.1-, DUTXR 3.1-folds.

Gene expression (RNAseq) analysis

Global gene expression profile (GEP) by RNA-sequencing was performed to identify and compare changes in gene expression induced by 3A.1 following single drug or 3A.1+TX combination regimens in PC3, PC3M, DU145, and DUTXR cell lines. GEP data from each treatment group and treatment time point were normalized to baseline (no-treatment) gene expression for the corresponding cell line, and heatmaps were generated (**Figure 3A**). A total of 492 genes were differentially expressed at 48 h post 3A.1 treatment above the significance threshold ($p<0.05$), while 442 and 672 genes were differentially expressed for the combination treatments 3A.1+DTX and CBZ+3A.1 (**Figure 3B**). The top differentially expressed genes

JPET Fast Forward. Published on December 23, 2021 as DOI: 10.1124/jpet.121.000898
This article has not been copyedited and formatted. The final version may differ from this version.

(DEGs) were identified for treatments involving 3A.1, viz. 3A.1 single-agent and 3A.1+DTX and 3A.1+CBZ treatments (**Table 3**). The top 10 upregulated DEGs between pre- (untreated; 0 h) *vs.* 48 h post-treatment, irrespective of treatment type (3A.1, 3A.1+DTX, 3A.1+CBX), were Hsp70, Hsp40, Hsp27, ARC, HMOX1, and BAG3, whereas top downregulated DEGs were MAT2A, RBM3, PAQR4 and PIGM (**Figure 3A and Table 3**). Additionally, upregulation of RPPH1 and downregulation of PSRC1, PCNA was observed after 3A.1 single-agent treatment.

IPA analysis performed based on the DEGs associated with 3A.1, single-agent and combination treatment (3A.1+DTX or 3A.1+CBZ) revealed activation Protein Ubiquitination Pathway (1.73E-19), Unfolded protein response (6.27E-15), NRF2-mediated Oxidative Stress Response (1.96E-11), Aldosterone Signaling in Epithelial Cells (1.08E-10), HIF1α signaling (1.59E-0.05 to 2.29E-0.05), BAG2 Signaling Pathway(1.70E-07), Cell Cycle: G2/M DNA Damage Checkpoint Regulation (1.74E-03), Kinetochore Metaphase Signaling Pathway (5.45E-03) and Mitotic Roles of Polo-Like Kinase (2.26E-02). Further, IPA predicted miRNA (miR-21-2) as the top upstream regulator based on the expression of downstream genes (**Figure 3C, Supplementary Figure 2A, I-III)**. Changes in gene expression induced by 3A.1-based dosing (single-agent and combination) regimens eventually triggered key pathways which may conquer drug resistance and increase treatment potency.

Gene expression (RNAseq) analysis in acquired TX-resistant mCRPC/NEPC line (DUTXR)

DUTXR (DU145 Taxane-resistant) treated with 3A.1, DTX, CBZ (single agent) and in combination for 48 h. GEP data from each treatment group were normalized to baseline gene expression for the corresponding cell line, and PCA plots were generated (**Figure 3D**). PCA plots based on post-treatment DEGs showed DU145 and DUTXR clustered in different groups (data not shown).

At FDR<0.05 and a fold change threshold <2,2178, genes were expressed differentially following 3A.1 single-agent treatment in DUTXR compared to 2303 and 2601 expressed differentially for the combination treatments of 3A.1+DTX and 3A.1+CBZ. Further, 1977 genes were found to be common between these three treatment groups indicating a possible influence of 3A.1 on these gene signatures. (**Figure 3D, Supplementary Table 1**).

JPET Fast Forward. Published on December 23, 2021 as DOI: 10.1124/jpet.121.000898
This article has not been copyedited and formatted. The final version may differ from this version.

IPA analysis was also performed based on the DEGs associated with 3A.1-based single-agent and combination treatments (3A.1+DTX or 3A.1+CBZ) on the DUTXR cell line. IPA predicted activation of similar pathways along with upregulation of Endoplasmic reticulum stress pathway and downregulation of PKR/PXR pathway, eNOS signaling, and oxidative phosphorylation pathways as unique for acquired resistant mCRPC (**Figure 3D, Supplementary Figure 2B**). IPA also identified upregulation of upstream regulator NUPR1, ATF4, NFE2l2, PPRC1, CREB1, POU5F1, EPAS1, XBP1, ATF3, KDM5B and downregulation of TRIB3 (**Figures 3D, Supplementary Figure 2B**).

***In silico* validation of the top DEGs using TCGA PRAD patient cohort**

We performed an *in silico* analysis of the top DEGs using prostate adenocarcinoma (PRAD-TCGA) patient GEP data available in the TCGA database. We explored the following groups: 1) All men with PCa; 2) AA (African American) vs. CA (Caucasian American) men with PCa and 3) high *vs.* low survivors. MAT2A expression was associated ($p<0.001$) with Gleason score (GS) and nodal metastasis status in prostate adenocarcinoma patients (PRAD-TCGA). MAT2A expression showed an increase with higher GS and in nodal metastasis N1compared to N0 (**Figure 4, I and II**). Concurrently, downregulation of MAT2A expression was observed following 3A.1 treatment in our mCRPC/NEPC cell lines (**Figure 4, III**). Additionally, TRA2B and SF1 were co-expressed highly ($r>0.7$) with MAT2A and were also associated with patient survival in PRAD patients (**Supplementary Figure 3**). PCNA expression was also increased with higher GS ($p<0.0001$), increased in nodal metastasis N1 compared to N0 and TP53 mutation status. Remarkably, 3A.1 treatment downregulated PCNA in our cell line models (**Figure 4A, IV-VI, and Table-3**). DDIT3, a pro-apoptotic factor that causes DNA damage along with transcription repression, was associated with poor survival ($p<0.0016$) in CA PCa patients. DDIT3 was also differentially expressed ($p<0.001$) in CA vs. AA patient group (**Figure 4A, VII**). Upregulation of this gene was noticed in our study following 3A.1 post-treatment. Further, PSRC1 ($p<0.001$) and RPPH1 ($p<0.009$) were also associated with higher GS in the PRAD-TCGA patient cohort (**Figure 4A, VIII-IX**).

Immunoblotting to confirm protein level changes

JPET Fast Forward. Published on December 23, 2021 as DOI: 10.1124/jpet.121.000898
This article has not been copyedited and formatted. The final version may differ from this version.

Based on the results of our RNA-seq expression data, IPA pathway analysis, and *in silico* (TCGA) patient data validation analyses, we selected the following top DEGs for immunoblotting in PCa cell lines i) Hsp70, Hsp-40, Hsp90, and Hsp27 (~8-, ~5-, ~4.5-fold), BAG3 upregulated and MAT2A (~2.5-fold) downregulated by RNAseq in 3A.1 single-agent and combination with DTX/CBZ treatment respectively); ii) MMPs– identified as upregulated (~3-fold) gene; iii) H2AX as an indicator of DNA damage and iv) HIF-α identified as important genes by IPA. Immunoblotting results showed consistently greater upregulation of HSPs and downregulation of MAT2A and MMPs following 3A.1 treatment compared to control (**Figure 4B**). Increased protein levels of Hsp70, HSP90, Hsp40, hsp27, and BAG3 after 3A.1 treatment, compared with control, provided operational validation of HSP upregulation mechanism, which is an indicator of 3A.1 treatment potency as a single agent and as well as in combination regimen with a taxane (DTX/CBZ). Both the combination (DTX+3A.1 and CBZ+3A.1) treatments decreased MMP9, MMP1 (except PC3), HIF1α, and MAT2A expression in all cell lines compared to untreated controls, as well as DTX and CBZ single treatment regimens (**Figure 4B**). A significant difference was observed in PCa cells treated with 3A.1 vs. control for the proteins encoded by HSPs, BAG3, H2AX, MAT2A, MMP-1, MMP9, **Figure 4C**. Densitometry showed MAT2A (2-3), MMP9 (2-5), and MMP1 (2-5) were downregulated while Hsp70 (2-17), Hsp40 (2-15) and Hsp27 (2-30), Hsp90 (2-14), BAG3 (2-40) and H2AX (2-40) were upregulated after 3A.1 post-treatment. Interestingly, since IPA analysis had predicted post 3A.1 treatment DNA damage in all cell lines, we also noticed post 3A.1 treatment H2AX upregulation. A marked decrease in HIF1α expression in PC3, PC3M and DU145 cells exposed to 3A.1 corroborated with the IPA finding. In contrast, HIF1α increased in 3A.1 in post-treated DUTXR cell lines (**Figure 4B and C**).

Validation of key pathways identified by IPA analysis

3A.1 treatment regulates Cell cycle checkpoints: Since cell cycle was significant among all IPA signaling pathways, we chose to validate by using *in vitro* assessment of cell population in each cell cycle checkpoint (G1/S and G2/M) following 3A.1 single-agent and TX (DTX and CBZ) combination treatment. PC-3, PC3M, DU145, and DUTXR cells were exposed to estimated IC_{50}, predicted DRI dose, and estimated

JPET Fast Forward. Published on December 23, 2021 as DOI: 10.1124/jpet.121.000898
This article has not been copyedited and formatted. The final version may differ from this version.

lowest-IC_{50} for each drug (3A.1, DTX, and CBZ). Treatment of all cell lines with 3A.1 resulted in apparent G1/S checkpoint arrest. Concurrently, a higher number of cells are arrested at G1/S following combination treatments compared to DTX or CBZ alone (**Figure 5A**). Treatment of cells with 3A.1+ taxane (DTX/CBZ) at IC_{50} increased the highest percentage of cells in the G1 phase ($p<0.05$) (**Figure 5A**, only DUTXR result shown), with a concomitant decrease in S and G2 populations, which supported the findings from our DEGs and IPA analyses.

Treatment causes DNA damage (Comet Assay): Our IPA analysis had predicted G2/M DNA Damage Checkpoint Regulation (1.74E-03). Therefore, the effect of 3A.1 treatment on DNA damage (strand breaks) was detected using a COMET assay in PC3, PC3M, DU145, and DUTXR cell lines treated with estimated IC_{50} (MTT) for 24 h. A comet appearance (PC3-2.7, PC3M-7.3, DU145-6.8, and DUTXR-6.7 fold comet area) was formed with damaged DNA fragments spreading from the center or in the tail) in all cell lines following 3A.1 treatment compared with control. Compared to a no-treatment control, the comet areas were: PC3 2.70-, PC3M 7.26-, DU145 6.78-, and DUTXR 6.77-fold; while the tail areas were - PC3 1.7-, PC3M 2.2-, DU145 2.5-, and DUTXR 1.4-fold. Furthermore, 3A.1 caused DNA damage in all mCRPC cell lines to various degrees. In PC3M (aggressive mCRPC/NEPC), and showed the highest degree of DNA strand breaks following treatment (**Figure 5B**)

Cell migration

PC3, PC3M, DU145, and DUTXR cells were exposed to single-dose 3A.1 at the calculated $IC_{50,}$ and TX+3A.1 combination at estimated IC_{50} predicted DRI dose and estimated lowest-IC_{50} for each drug for 24 and 48 h to examine the effect of different dose regimens on the cell migration as measured by using Scratch/wound healing assay. Results revealed that combination treatment (DTX+3A.1 and CBZ+3A.1) has a higher effect in reducing cell migration in prostate cancer cell lines ($p<0.05$). Notably, the predicted DRI dose showed the highest degree of reduction in cell migration (~3 folds) (**Figure 5C, Supplementary Figure 4**).

JPET Fast Forward. Published on December 23, 2021 as DOI: 10.1124/jpet.121.000898
This article has not been copyedited and formatted. The final version may differ from this version.

DISCUSSION

PCa is the second leading cause of non-cutaneous cancer deaths in the United States (www.cancer.org). Standard treatments include prostatectomy and/or radiation with or without hormonal manipulation for localized prostate cancer(Magnan *et al.*, 2015; Hamdy *et al.*, 2016). However, many patients eventually develop resistance to androgen deprivation therapy (ADT), *i.e.,* non-metastatic castration-resistant prostate cancer (nmCRPC) and metastatic CRPC (mCRPC/NEPC) (Yuan *et al.*, 2007; Sun *et al.*, 2009; Scher *et al.*, 2015). Chemotherapy with DTX/CBZ alone or in combination with bevacizumab, thalidomide, *and* prednisone increases median overall survival (OS) by less than a year and represents the primary treatment option for recurrent prostate cancers(Bai *et al.*, n.d.; De Bono *et al.*, 2010). Innovative immunotherapy approaches have been shown to increase OS in patients with hormone-refractory metastatic prostate cancer by 4-5 months(Hall *et al.*, 2011). However, the effectiveness of most chemotherapeutic agents is limited by non-target tissue toxicity, heterogeneous nature of tumor among patients, and development of drug resistance(Tannock, 2014). Therefore, effective chemotherapeutic strategies for treating mCRPC/NEPC are needed to delay disease progression and improve survival.

Combination chemotherapy is used widely to treat various malignancies, including PCa. The principal goals of the combination therapy against cancer are to achieve a synergistic effect at lower doses, delay or eliminate the development of chemoresistance, and achieve greater therapeutic responses(Xu and Qiu, n.d.). The synergistic drug interaction could reduce the overall dose of taxane drugs below its maximum tolerated dose (MTD), reducing the risk of serious side effects, and developing well-tolerated chemotherapy regimen(Pannu *et al.*, 2011; Wang *et al.*, 2015; Mukhtar *et al.*, 2016).

Our previous studies suggested that the Andrographolide analogue 3A.1 exhibited anticancer efficacy against colorectal cancer by inducing apoptosis and inhibition of cell migration(Kansom *et al.*, 2019). Other studies have reported that 3A.1 exhibited anticancer activity in colon cancer by activating PARP, H2AX, P53, Bax, and inhibiting MMP7, Cox-2, Cas-3, CDK6, CyclinD1, and Wnt/β-catenin proteins through DNA damage, apoptosis, and inhibition of cell growth(Reabroi *et al.*, 2018). However, the MOA is not

JPET Fast Forward. Published on December 23, 2021 as DOI: 10.1124/jpet.121.000898
This article has not been copyedited and formatted. The final version may differ from this version.

understood fully. In this study, we demonstrated that 3A.1 single drug and combination treatment with DTX/CBZ may be used to achieve increased sensitivity compared to conventional high-dose Taxane drug schedules to overcome drug resistance in mCRPC/NEPC. Further, our current study also focused on comprehensive gene expression (RNA-seq) and key pathway analysis to gain mechanistic insights into 3A.1 activity.

The top ten DEGs associated with 3A.1treatment include upregulation of heat shock proteins/HSPs, ARC, BAG3, HMOX1, RPPH1, and down-regulation of MAT2A, PSRC1, and PCNA. Additionally, down-regulation of MAT2A was also associated with improved patient survival in TCGA PCa patients. Further, PCNA, DDIT3, PSRC1, and RPPH1 were also associated ($p<0.001$) with patient GS and nodal metastasis in PCa patients.

HSPs play a crucial role in several biological processes involved in the maintenance of cellular protein homeostasis in a normal cell as wells as in cancer cells, including protein folding, cellular proliferation, differentiation, survival, metastasis, invasion, and angiogenesis(Christians *et al.*, 2003; Saibil, 2013; Shrestha *et al.*, 2016). Upregulation of HSPs induces p53 signaling, which causes cell cycle arrest and apoptosis(Harris and Levine, 2005). In colon cancer cells, HSPs play an important role by activation of p53 during Andrographolide (mother compound of 3A.1) treatment(Sato *et al.*, 2018). Further, AR signaling plays a crucial role in the development of mCRPC, and Andrographolide prevents the binding of Hsp90/Hsp70 chaperon to AR, resulting in proteasome-mediated AR degradation(Liu *et al.*, 2011; Hessenkemper and Baniahmad, 2013). HSPs inhibit an inter-domain interaction necessary for transcriptional activity of AR and regulate cellular concentration, solubility, and degradation of AR(Eftekharzadeh *et al.*, 2019). Additionally, upregulation of HSPs also enables cancer cells to switch from an AR+ to an AR- disease to restore AR-dependence(Formaggio *et al.*, 2021). Therefore, upregulation of HSPs is beneficial to overcome resistance and aggressiveness, and our western blotting data confirmed our transcriptomic analysis findings where 3A.1 single-agent and combination treatment with DTX/CBZ increased HSP70b1, HSP40, Hsp27, and HSP90α protein expression in mCRPC/NEPC cell lines.

JPET Fast Forward. Published on December 23, 2021 as DOI: 10.1124/jpet.121.000898
This article has not been copyedited and formatted. The final version may differ from this version.

Additionally, there is evidence supporting the crosstalk and functional overlap of the stress responses modulated by HSF1 (transcription factor regulating the expression of HSPs) and NRF2, which activate ubiquitin proteasome system (UPS), oxidative stress pathway to regulate cancer progression along with upregulation of HMOX1 to regulates cell cycle and DNA damage(Saibil, 2013; Quah *et al.*, 2021). Here, IPA pathway prediction corroborates with this finding, we identified NEF2 mediated oxidative stress response pathway activation and UPS pathway after 3A.1 treatment.

Interaction of BAG3 with Hsp70/40 is seen as a key regulator of cancer cell signaling. Studies suggested PCa patients showed high-grade tumors had low levels of BAG3 and high expression associated with favorable outcome(Staibano *et al.*, 2010). Additionally, BAG3 overexpression results in decreased migration and adhesion(Kassis *et al.*, 2006). We found Bag 3 upregulation after 3A.1 treatment, which may increase treatment efficacy in combination with standard drugs (DTX/CBZ). Further, in our study HMOX1, was upregulated after treatment. Earlier studies have also suggested that HMOX1 is upregulated by Andrographolide treatment(Staibano *et al.*, 2010). Further, over-expression of HMOX1 decreased the proliferation, migration, and the invasive potential of PCa cells by down-regulating MMP9 expression and DNA damage(Gueron *et al.*, 2009). Additionally, concurrent to our observation (cell migration, cell cycle, comet, and immunoblotting analysis), 3A.1 treatment has also been shown to reduce MMPs expression(Reabroi *et al.*, 2018). Our IPA analysis predicted inhibition of mir21 and MMP9. Previously, it has been shown that miR21 overexpressed in recurrent prostate tumors and is associated with increased expression of MMP9 and cell invasion(Leite *et al.*, 2015). This indicates crosstalk between miR21 and MMP9 vis-à-vis cell migration, which 3A.1 potentially inhibits.

MAT2A plays a crucial role in various cancer progression including PCa(Maldonado *et al.*, 2018; Munkley *et al.*, 2018). Inhibition of MAT2A gene expression repressed the growth of human PCa(Ma *et al.*, 2008). Several miRNAs, including mir-21, also regulate MAT2A post-transcriptionally, and inhibition of mir-21 by the anticancer drug was shown to suppress MAT2A mRNA level in liver cancer cells leading to growth arrest and apoptosis(Lo *et al.*, 2013). In our study, MAT2A was the top downregulated gene and protein

JPET Fast Forward. Published on December 23, 2021 as DOI: 10.1124/jpet.121.000898
This article has not been copyedited and formatted. The final version may differ from this version.

following 3A.1 treatment. Further, IPA analysis exhibited that post 3A.1 treatment also inhibited mir21 in our study, which concurred with the previous finding. In addition, activation of ubiquitination pathway by inhibition of MAT2A identified by post 3A.1 treatment corroborated with an earlier study showing MAT2A-induced cell proliferation in human hepatocellular cancer(Yang *et al.*, 2015).

Baseline DDIT3 expression was higher in AI-mCRPC cell lines and TCGA PCa patient group with poor survival. Further, following 3A.1+CBZ treatment showed >3.5-fold upregulation of DDIT3 in PCa cell lines. DDIT3 is a regulator of cell cycle arrest and apoptosis in response to ER stress(Yamaguchi and Wang, 2004; Ohoka *et al.*, 2005). Moreover, DDIT3 inhibits the canonical Wnt signaling pathway by binding to TCF/LEF following DNA damage and represses its transcriptional activity(Bantis *et al.*, 2004; Reabroi *et al.*, 2018).

H2AX protein upregulation following 3A.1 treatment is an indication of DNA breaks repair that we confirmed using COMET assays. Earlier studies have shown similar findings of 3A.1 treatment associated DNA damage and H2AX expression(Reabroi *et al.*, 2018). Moreover, DNA damage causes activation of P53 mediated cell cycle arrest and apoptosis(Harris and Levine, 2005). Earlier studies showed that 3A.1 induces apoptosis by activating caspase3 and arrests the cell cycle at sub G0/G1 phase by DNA damage through PARP-1 and p53 activation in cholangio-carcinoma(Reabroi *et al.*, 2018). In our study, IPA analysis identified DNA damage pathway and p53 signaling activation whereas *in vitro* assays showed 3A.1 treatment causes DNA damage, G/S cell cycle arrest, and increased apoptosis in mCRPC/NEPC.

PCNA is a nuclear protein and recognized as a marker for cell proliferation, cell cycle G1/S regulator, DNA damage repair and correlated significantly with the degree of GS(Sulik and Guzińska-Ustymowicz, 2002; Wang *et al.*, 2010; Glover *et al.*, 2017). Andrographolides show induced cell proliferation in cancer tissue by inhibiting the expression of PCNA(Chang *et al.*, 2014). Our *in silico* validation using TCGA patient cohort demonstrated that higher PCNA expression was observed in higher GS, nodal metastasis status, and TP53/p53 mutation groups compared to less severe subgroups. Further, we observed that 3A.1 treatment downregulated PCNA expression and caused DNA damage, cell cycle regulation, along with p53

activation. PSRC1 has been shown to influence cancer cell proliferation and tumor growth through p53(Mangé *et al.*, 2012). Further, TCGA PRAD patient cohort validation showed that higher expression of PSRC1 was associated with high GS in PCa patients.

Taken together, our results showed 3A.1 treatment influences key pathways responsible for DNA damage, cell proliferation, migration, invasion, differentiation, transformation, metastasis, and apoptosis, indicating a probable basis for the increased potency of 3A.1 treatment as a single-agent and in combination with DTX/CBZ over conventional taxane therapy. Additionally, the top genes HSPs, MMP1, MMP9, HIF-α, and MAT2A were expressed differentially between cell lines and patients representing AA vs. EA patients and significantly associated with patient's survival, nodal metastasis, and GS. This indicates the potential benefits of using 3A.1 to address racial disparity in PCa patients since AA men have a higher incidence, higher mortality rate, and more aggressiveness compared to EA men.

Our results thus provide key insights into the 3A.1 response mechanism in PCa. We understand that using a limited number of cell lines and patient datasets as model systems for aggressive PCa is a limitation. Therefore, larger-scale studies involving a wider panel of cell lines, *in vivo*, and clinical samples are required to validate the pharmacogenomics of 3A.1 response and to establish 3A.1 as a viable combination treatment approach to circumvent the challenge of drug resistance. Nevertheless, these data suggest that 3A.1 treatment may provide a novel treatment strategy that combines its favorable properties with the benefits of combination treatments in controlling aggressive PCa.

JPET Fast Forward. Published on December 23, 2021 as DOI: 10.1124/jpet.121.000898
This article has not been copyedited and formatted. The final version may differ from this version.

ACKNOWLEDGEMENT

TMG was supported by the Department of Drug Discovery & Development, Harrison School of Pharmacy.

We thankfully acknowledge the Center for Pharmacogenomics and Single-Cell Omics, Auburn University, for support with analysis.

JPET Fast Forward. Published on December 23, 2021 as DOI: 10.1124/jpet.121.000898
This article has not been copyedited and formatted. The final version may differ from this version.

AUTHOR CONTRIBUTIONS

Participated in Research design: Taraswi Mitra Ghosh, Teeratas Kansom, and Robert D. Arnold

Conducted Experiments: Taraswi Mitra Ghosh, Teeratas Kansom (part of cytotoxicity, cell morphological study, Immunoblotting), Ahmed S. Alnaim (cell morphological study), Joshua Davis, Shanese L. Jasper, Chu Zhang (assisted with cell culture maintenance and studies), Aedan Bird (assisted with Immunoblotting)

Performed data analysis: Taraswi Mitra Ghosh, Suman Mazumder, Amit K Mitra

Wrote or contributed to the writing of the manuscript: Taraswi Mitra Ghosh, Teeratas Kansom, Praneet Opanasopit, Amit K Mitra, and Robert D. Arnold

Supervised the project: Robert D. Arnold

FINANCIAL DISCLOSURE

The authors declare that they have no conflicts of interest with the contents of this article.

REFERENCES

Aljuffali IA, Mock JN, Costyn LJ, Nguyen H, Nagy T, Cummings BS, and Arnold RD (2011) Enhanced antitumor activity of low-dose continuous administration schedules of topotecan in prostate cancer. *Cancer Biol Ther* **12**:407–20.

Amin A, Gali-Muhtasib H, Ocker M, and Schneider-Stock R (2009) Overview of major classes of plant-derived anticancer drugs. *Int J Biomed Sci* **5**:1–11.

Annala M, Vandekerkhove G, Khalaf D, Taavitsainen S, Beja K, Warner EW, Sunderland K, Kollmannsberger C, Eigl BJ, Finch D, Oja CD, Vergidis J, Zulfiqar M, Azad AA, Nykter M, Gleave ME, Wyatt AW, and Chi KN (2018) Circulating Tumor DNA Genomics Correlate with Resistance to Abiraterone and Enzalutamide in Prostate Cancer. *Cancer Discov* **8**:444–457.

Bai S, Zhang BY, and Dong Y (n.d.) Impact of taxanes on androgen receptor signaling. *Asian J Androl* **21**:249–252.

Bantis A, Giannopoulos A, Gonidi M, Liossi A, Aggelonidou E, Petrakakou E, Athanassiades P, and Athanassiadou P (2004) Expression of p120, Ki-67 and PCNA as proliferation biomarkers in imprint smears of prostate carcinoma and their prognostic value. *Cytopathology* **15**:25–31.

Chandrashekar DS, Bashel B, Balasubramanya SAH, Creighton CJ, Ponce-Rodriguez I, Chakravarthi BVSK, and Varambally S (2017) UALCAN: A Portal for Facilitating Tumor Subgroup Gene Expression and Survival Analyses. *Neoplasia* **19**:649–658.

Chang C-C, Duann Y-F, Yen T-L, Chen Y-Y, Jayakumar T, Ong E-T, and Sheu J-R (2014) Andrographolide, a Novel NF-κB Inhibitor, Inhibits Vascular Smooth Muscle Cell Proliferation and Cerebral Endothelial Cell Inflammation. *Acta Cardiol Sin* **30**:308–15.

Chou TC, and Talalay P (1984) Quantitative analysis of dose-effect relationships: the combined effects of multiple drugs or enzyme inhibitors. *Adv Enzyme Regul* **22**:27–55.

Christians ES, Zhou Q, Renard J, and Benjamin IJ (2003) Heat shock proteins in mammalian development. *Semin Cell Dev Biol* **14**:283–90.

Chun JY, Tummala R, Nadiminty N, Lou W, Liu C, Yang J, Evans CP, Zhou Q, and Gao AC (2010) Andrographolide, an herbal medicine, inhibits interleukin-6 expression and suppresses prostate cancer cell growth. *Genes Cancer* **1**:868–76.

Corn PG, Agarwal N, Araujo JC, and Sonpavde G (2019) Taxane-based Combination Therapies for Metastatic Prostate Cancer. *Eur Urol Focus* **5**:369–380.

Dai Y, Chen S-R, Chai L, Zhao J, Wang Yitao, and Wang Ying (2019) Overview of pharmacological activities of Andrographis paniculata and its major compound andrographolide. *Crit Rev Food Sci Nutr* **59**:S17–S29.

Darshan MS, Loftus MS, Thadani-Mulero M, Levy BP, Escuin D, Zhou XK, Gjyrezi A, Chanel-Vos C, Shen R, Tagawa ST, Bander NH, Nanus DM, and Giannakakou P (2011) Taxane-induced blockade to nuclear accumulation of the androgen receptor predicts clinical responses in metastatic prostate cancer. *Cancer Res* **71**:6019–29.

De Bono JS, Oudard S, Ozguroglu M, Hansen S, MacHiels J-PP, Kocak I, Gravis G, Bodrogi I, MacKenzie MJ, Shen L, Roessner M, Gupta S, Sartor AO, and TROPIC Investigators (2010) Prednisone plus cabazitaxel or mitoxantrone for metastatic castration-resistant prostate cancer progressing after docetaxel treatment: a randomised open-label trial. *Lancet (London, England)* **376**:1147–54, Elsevier Ltd.

Demain AL, and Vaishnav P (2011) Natural products for cancer chemotherapy. *Microb Biotechnol* **4**:687–99.

Duran GE, Wang YC, Francisco EB, Rose JC, Martinez FJ, Coller J, Brassard D, Vrignaud P, and Sikic BI (2015) Mechanisms of resistance to cabazitaxel. *Mol Cancer Ther* **14**:193–201.

Eftekharzadeh B, Banduseela VC, Chiesa G, Martínez-Cristóbal P, Rauch JN, Nath SR, Schwarz DMC, Shao H, Marin-Argany M, Di Sanza C, Giorgetti E, Yu Z, Pierattelli R, Felli IC, Brun-Heath I, García J, Nebreda ÁR, Gestwicki JE, Lieberman AP, and Salvatella X (2019) Hsp70 and Hsp40 inhibit an inter-domain interaction necessary for transcriptional activity in the androgen receptor. *Nat Commun* **10**:3562.

Forestier-Román IS, López-Rivas A, Sánchez-Vázquez MM, Rohena-Rivera K, Nieves-Burgos G, Ortiz-Zuazaga H, Torres-Ramos CA, and Martínez-Ferrer M (2019) Andrographolide induces DNA damage in prostate cancer cells. *Oncotarget* **10**:1085–1101.

Formaggio N, Rubin MA, and Theurillat J-P (2021) Loss and revival of androgen receptor signaling in advanced prostate cancer. *Oncogene* **40**:1205–1216.

Galletti G, Leach BI, Lam L, and Tagawa ST (2017) Mechanisms of resistance to systemic therapy in metastatic castration-resistant prostate cancer. *Cancer Treat Rev* **57**:16–27.

Glover M, Soni S, Ren Q, Maclennan GT, Fu P, and Gupta S (2017) Influence of chronic inflammation on Bcl-2 and PCNA expression in prostate needle biopsy specimens. *Oncol Lett* **14**:3927–3934.

Gueron G, De Siervi A, Ferrando M, Salierno M, De Luca P, Elguero B, Meiss R, Navone N, and Vazquez ES (2009) Critical role of endogenous heme oxygenase 1 as a tuner of the invasive potential of prostate cancer cells. *Mol Cancer Res* **7**:1745–55.

Hall SJ, Klotz L, Pantuck AJ, George DJ, Whitmore JB, Frohlich MW, and Sims RB (2011) Integrated safety data from 4 randomized, double-blind, controlled trials of autologous cellular immunotherapy with sipuleucel-T in patients with prostate cancer. *J Urol* **186**:877–81.

Hamdy FC, Donovan JL, Lane JA, Mason M, Metcalfe C, Holding P, Davis M, Peters TJ, Turner EL, Martin RM, Oxley J, Robinson M, Staffurth J, Walsh E, Bollina P, Catto J, Doble A, Doherty A, Gillatt D, Kockelbergh R, Kynaston H, Paul A, Powell P, Prescott S, Rosario DJ, Rowe E, Neal DE, and ProtecT Study Group (2016) 10-Year Outcomes after Monitoring, Surgery, or Radiotherapy for Localized Prostate Cancer. *N Engl J Med* **375**:1415–1424.

Harris SL, and Levine AJ (2005) The p53 pathway: positive and negative feedback loops. *Oncogene* **24**:2899–908.

Hessenkemper W, and Baniahmad A (2013) Targeting heat shock proteins in prostate cancer. *Curr Med Chem* **20**:2731–40.

Hwang C (2012) Overcoming docetaxel resistance in prostate cancer: a perspective review. *Ther Adv Med Oncol* **4**:329–40.

Kansom T, Sajomsang W, Saeeng R, Charoensuksai P, Opanasopit P, and Tonglairoum P (2018) Apoptosis Induction and Antimigratory Activity of Andrographolide Analog (3A.1)-Incorporated Self-Assembled Nanoparticles in Cancer Cells. *AAPS PharmSciTech* **19**:3123–3133.

Kansom T, Sajomsang W, Saeeng R, Rojanarata T, Ngawhirunpat T, Patrojanasophon P, and Opanasopit P (2019) Fabrication and characterization of andrographolide analogue (3A. 1) nanosuspensions stabilized by amphiphilic chitosan derivatives for colorectal cancer therapy. *J Drug Deliv Sci Technol* **54**:101287, Elsevier.

Kassis JN, Guancial EA, Doong H, Virador V, and Kohn EC (2006) CAIR-1/BAG-3 modulates cell adhesion and migration by downregulating activity of focal adhesion proteins. *Exp Cell Res* **312**:2962–71.

Krämer A, Green J, Pollard J, and Tugendreich S (2014) Causal analysis approaches in Ingenuity

Pathway Analysis. *Bioinformatics* **30**:523–30.

Leite KRM, Reis ST, Viana N, Morais DR, Moura CM, Silva IA, Pontes J, Katz B, and Srougi M (2015) Controlling RECK miR21 Promotes Tumor Cell Invasion and Is Related to Biochemical Recurrence in Prostate Cancer. *J Cancer* **6**:292–301.

Liu C, Nadiminty N, Tummala R, Chun JY, Lou W, Zhu Y, Sun M, Evans CP, Zhou Q, and Gao AC (2011) Andrographolide targets androgen receptor pathway in castration-resistant prostate cancer. *Genes Cancer* **2**:151–9.

Lo T-F, Tsai W-C, and Chen S-T (2013) MicroRNA-21-3p, a berberine-induced miRNA, directly down-regulates human methionine adenosyltransferases 2A and 2B and inhibits hepatoma cell growth. *PLoS One* **8**:e75628.

Ma C, Ci M, Yoshioka M, Mayumi Y, Boivin A, André B, Belleau P, Pascal B, Gan L, Lin G, Takase Y, Yasukazu T, Labrie F, Fernand L, St-Amand J, and Jonny S-A (2008) Prostate-specific genes and their regulation by dihydrotestosterone. *Prostate* **68**:241–54.

Machioka K, Izumi K, Kadono Y, Iwamoto H, Naito R, Makino T, Kadomoto S, Natsagdorj A, Keller ET, Zhang J, and Mizokami A (2018) Establishment and characterization of two cabazitaxel-resistant prostate cancer cell lines. *Oncotarget* **9**:16185–16196.

Magnan S, Zarychanski R, Pilote L, Bernier L, Shemilt M, Vigneault E, Fradet V, and Turgeon AF (2015) Intermittent vs Continuous Androgen Deprivation Therapy for Prostate Cancer: A Systematic Review and Meta-analysis. *JAMA Oncol* **1**:1261–9.

Maldonado LY, Arsene D, Mato JM, and Lu SC (2018) Methionine adenosyltransferases in cancers: Mechanisms of dysregulation and implications for therapy. *Exp Biol Med (Maywood)* **243**:107–117.

Mangé A, Lacombe J, Bascoul-Mollevi C, Jarlier M, Lamy P-J, Rouanet P, Maudelonde T, and Solassol J (2012) Serum autoantibody signature of ductal carcinoma in situ progression to invasive breast cancer. *Clin Cancer Res* **18**:1992–2000.

Mukhtar E, Adhami VM, Siddiqui IA, Verma AK, and Mukhtar H (2016) Fisetin Enhances Chemotherapeutic Effect of Cabazitaxel against Human Prostate Cancer Cells. *Mol Cancer Ther* **15**:2863–2874.

Munkley J, Maia TM, Ibarluzea N, Livermore KE, Vodak D, Ehrmann I, James K, Rajan P, Barbosa-Morais NL, and Elliott DJ (2018) Androgen-dependent alternative mRNA isoform expression in prostate cancer cells. *F1000Research* **7**:1189.

Nateewattana J, Dutta S, Reabroi S, Saeeng R, Kasemsook S, Chairoungdua A, Weerachayaphorn J, Wongkham S, and Piyachaturawat P (2014) Induction of apoptosis in cholangiocarcinoma by an andrographolide analogue is mediated through topoisomerase II alpha inhibition. *Eur J Pharmacol* **723**:148–55.

Nateewattana J, Saeeng R, Kasemsook S, Suksen K, Dutta S, Jariyawat S, Chairoungdua A, Suksamrarn A, and Piyachaturawat P (2013) Inhibition of topoisomerase II α activity and induction of apoptosis in mammalian cells by semi-synthetic andrographolide analogues. *Invest New Drugs* **31**:320–32.

Ohoka N, Yoshii S, Hattori T, Onozaki K, and Hayashi H (2005) TRB3, a novel ER stress-inducible gene, is induced via ATF4-CHOP pathway and is involved in cell death. *EMBO J* **24**:1243–55.

Oudard S, Fizazi K, Sengeløv L, Daugaard G, Saad F, Hansen S, Hjälm-Eriksson M, Jassem J, Thiery-Vuillemin A, Caffo O, Castellano D, Mainwaring PN, Bernard J, Shen L, Chadjaa M, and Sartor O (2017) Cabazitaxel Versus Docetaxel As First-Line Therapy for Patients With Metastatic Castration-Resistant Prostate Cancer: A Randomized Phase III Trial-FIRSTANA. *J Clin Oncol* **35**:3189–3197.

Pannu V, Karna P, Sajja HK, Shukla D, and Aneja R (2011) Synergistic antimicrotubule therapy for

prostate cancer. *Biochem Pharmacol* **81**:478–87.

Pawar A, Rajalakshmi S, Mehta P, Shaikh K, and Bothiraja C (2016) Strategies for formulation development of andrographolide. *RSC Adv* **6**:69282–69300, Royal Society of Chemistry.

Quah SY, Wong CC, Wong HC, Ho KL, Abdul Manan N, Deb PK, Sagineedu SR, and Stanslas J (2021) Microarray-based identification of differentially expressed genes associated with andrographolide derivatives-induced resistance in colon and prostate cancer cell lines. *Toxicol Appl Pharmacol* **425**:115605.

Quinn DI, Sandler HM, Horvath LG, Goldkorn A, and Eastham JA (2017) The evolution of chemotherapy for the treatment of prostate cancer. *Ann Oncol Off J Eur Soc Med Oncol* **28**:2658–2669.

Reabroi S, Chairoungdua A, Saeeng R, Kasemsuk T, Saengsawang W, Zhu W, and Piyachaturawat P (2018) A silyl andrographolide analogue suppresses Wnt/β-catenin signaling pathway in colon cancer. *Biomed Pharmacother* **101**:414–421.

Ritchie ME, Phipson B, Wu D, Hu Y, Law CW, Shi W, and Smyth GK (2015) limma powers differential expression analyses for RNA-sequencing and microarray studies. *Nucleic Acids Res* **43**:e47.

Saibil H (2013) *No Title*.

Sato H, Hiraki M, Namba T, Egawa N, Baba K, Tanaka T, and Noshiro H (2018) Andrographolide induces degradation of mutant p53 via activation of Hsp70. *Int J Oncol* **53**:761–770.

Scher HI, Fizazi K, Saad F, Taplin M-E, Sternberg CN, Miller K, de Wit R, Mulders P, Chi KN, Shore ND, Armstrong AJ, Flaig TW, Fléchon A, Mainwaring P, Fleming M, Hainsworth JD, Hirmand M, Selby B, Seely L, de Bono JS, and AFFIRM Investigators (2012) Increased survival with enzalutamide in prostate cancer after chemotherapy. *N Engl J Med* **367**:1187–97.

Scher HI, Solo K, Valant J, Todd MB, and Mehra M (2015) Prevalence of Prostate Cancer Clinical States and Mortality in the United States: Estimates Using a Dynamic Progression Model. *PLoS One* **10**:e0139440.

Seca AML, and Pinto DCGA (2018) Plant Secondary Metabolites as Anticancer Agents: Successes in Clinical Trials and Therapeutic Application. *Int J Mol Sci* **19**.

Shrestha L, Bolaender A, J. Patel H, and Taldone T (2016) Heat Shock Protein (HSP) Drug Discovery and Development: Targeting Heat Shock Proteins in Disease. *Curr Top Med Chem* **16**:2753–2764, Bentham Science Publishers Ltd.

Staibano S, Mascolo M, Di Benedetto M, Vecchione ML, Ilardi G, Di Lorenzo G, Autorino R, Salerno V, Morena A, Rocco A, Turco MC, and Morelli E (2010) BAG3 protein delocalisation in prostate carcinoma. *Tumour Biol* **31**:461–9.

Sulik M, and Guzińska-Ustymowicz K (2002) Expression of Ki-67 and PCNA as proliferating markers in prostate cancer. *Rocz Akad Med Bialymst* **47**:262–9.

Sun Y, Niu J, and Huang J (2009) Neuroendocrine differentiation in prostate cancer. *Am J Transl Res* **1**:148–62.

Tannock IF (2014) Words of wisdom. Re: Intratumor heterogeneity and branched evolution revealed by multiregion sequencing. *Eur Urol* **65**:846–7.

Varma A, Padh H, and Shrivastava N (2011) Andrographolide: a new plant-derived antineoplastic entity on horizon. *Evid Based Complement Alternat Med* **2011**:815390.

Wang C-D, Huang J-G, Gao X, Li Y, Zhou S-Y, Yan X, Zou A, Chang J-L, Wang Y-S, Yang G-X, and He G-Y (2010) Fangchinoline induced G1/S arrest by modulating expression of p27, PCNA, and

cyclin D in human prostate carcinoma cancer PC3 cells and tumor xenograft. *Biosci Biotechnol Biochem* **74**:488–93.

Wang P, Henning SM, Heber D, and Vadgama J V (2015) Sensitization to docetaxel in prostate cancer cells by green tea and quercetin. *J Nutr Biochem* **26**:408–15.

Wong HC, Sagineedu SR, Lajis NH, Loke SC, and Stanslas J (2011) Andrographolide induces cell cycle arrest and apoptosis in PC-3 prostate cancer cells. *African J Pharm Pharmacol* **5**:225–233, Academic Journals.

Xu J, and Qiu Y (n.d.) Current opinion and mechanistic interpretation of combination therapy for castration-resistant prostate cancer. *Asian J Androl* **21**:270–278.

Yadav SS, Li J, Stockert JA, Herzog B, O'Connor J, Garzon-Manco L, Parsons R, Tewari AK, and Yadav KK (2017) Induction of Neuroendocrine Differentiation in Prostate Cancer Cells by Dovitinib (TKI-258) and its Therapeutic Implications. *Transl Oncol* **10**:357–366.

Yamaguchi H, and Wang H-G (2004) CHOP is involved in endoplasmic reticulum stress-induced apoptosis by enhancing DR5 expression in human carcinoma cells. *J Biol Chem* **279**:45495–502.

Yang H-B, Xu Y-Y, Zhao X-N, Zou S-W, Zhang Y, Zhang M, Li J-T, Ren F, Wang L-Y, and Lei Q-Y (2015) Acetylation of MAT IIα represses tumour cell growth and is decreased in human hepatocellular cancer. *Nat Commun* **6**:6973.

Ye L, Wang T, Tang L, Liu W, Yang Z, Zhou J, Zheng Z, Cai Z, Hu M, and Liu Z (2011) Poor oral bioavailability of a promising anticancer agent andrographolide is due to extensive metabolism and efflux by P-glycoprotein. *J Pharm Sci* **100**:5007–17.

Yuan T-C, Veeramani S, and Lin M-F (2007) Neuroendocrine-like prostate cancer cells: neuroendocrine transdifferentiation of prostate adenocarcinoma cells. *Endocr Relat Cancer* **14**:531–47.

JPET Fast Forward. Published on December 23, 2021 as DOI: 10.1124/jpet.121.000898
This article has not been copyedited and formatted. The final version may differ from this version.

FOOTNOTES

Funding

This work was supported in part by funding from U54-MD007585-26 (NIH/NIMHD), U54 639 CA118623 (NIH/NCI), and Department of Defense Grants (PC170315P1 and PC190741). Partial work was also assisted by the Thailand Research Sciences and Innovation (TSRI) through the Royal Golden Jubilee Ph.D. program (PHD/0077/2558).

Abbreviations

3A.1	**semi-synthetic andrographolide analogue**
AA	**African American**
ADT	**Androgen deprivation therapy**
AG	**andrographolide**
AR	**androgen receptor**
CA	**Caucasian American**
CI	**combination Index**
CBZ	**cabazitaxel**
DTX	**docetaxel**
DEG	**differentially expressed gene**
DMSO	**dimethyl sulfoxide**
DRI	**dose reduction index**
DU145	**EA origin castration-resistant human prostate cancer cells**
DUTXR	**EA origin DU145 taxane resistant human prostate cancer cells**
EA	**European American or Caucasian**
FBS	**fetal bovine serum**
GEP	**gene expression profiling**
H	**hour(s)**
IC_{50}	**half maximal inhibitory concentration**
IPA	**ingenuity pathway analysis**
mCRPC	**metastatic, castration-resistant prostate cancer**
mRNA	**messenger RNA**

JPET Fast Forward. Published on December 23, 2021 as DOI: 10.1124/jpet.121.000898
This article has not been copyedited and formatted. The final version may differ from this version.

miRNA	**micro RNA**
MOA	**mechanism of action**
MTT	**3-(4, 5-dimethylthiazol-2-yl)-2,5-diphenyltetrazolium bromide**
NOR	**normal**
OS	**overall survival**
PBS	**phosphate buffered saline**
PC-3	**castration-resistant human prostate cancer cells**
PC3M	**highly metastatic PC3 human prostate cancer cells**
PCa	**prostate cancer**
PRAD	**prostate adenocarcinoma**
RNA-Seq	**RNA sequencing**
RD	**reduced dose**
SRB	**sulforhodamine B**
TCA	**trichloroacetic acid**
TBS	**tris buffered saline**
TRIS	**tris (hydroxymethyl) aminomethane buffer**
TCGA	**The Cancer Genome Atlas**

JPET Fast Forward. Published on December 23, 2021 as DOI: 10.1124/jpet.121.000898
This article has not been copyedited and formatted. The final version may differ from this version.

FIGURE LEGENDS

Figure 1. Structure and *In vitro* effect of single-agent andrographolide analogue (3A.1)/Docetaxel (DTX)/ Cabazitaxel (CBZ) treatment on the growth of human aggressive prostate cells.

A) Structure of 3A.1, DTX, and CBZ

B) *In vitro* cytotoxicity was assessed following 48 h of 3A.1, DTX, and CBZ treatment in PC3, PC3M, DU145, DUTXR cell lines using mitochondrial activity (3-(4, 5-Dimethylthiazol-2-yl)-2,5-diphenyltetrazolium bromide or MTT assay) at increasing drug concentrations. Bar graph show percent survival compared with control at increasing concentrations of DTX, CBZ, and 3A.1 single agent 48 h treatment in PC3, PC3M, DU145, and DUTXR cell lines. (* = $p \leq 0.05$).

C) Bar graphs represent the AUC values for all cell lines treated with the DTX, CBZ, and 3A.1 as a single-agent. All cell lines exhibited inter-individual variation in response. (* = $p \leq 0.05$).

Figure 2. Effect of combination treatment andrographolide analogue (3A.1) and taxanes (Docetaxel (DTX), Cabazitaxel (CBZ)) on the growth of human aggressive prostate cells *in vitro*.

A) *In vitro* cytotoxicity was assessed following 48 h of 3A.1+DTX and 3A.1+CBZ treatment in PC3, PC3M, DU145, DUTXR cell lines using mitochondrial activity (3-(4, 5-Dimethylthiazol-2-yl)-2,5-diphenyltetrazolium bromide or MTT assay) at increasing drug concentrations. Bar graphs represent the dose reduction (Reduce Dose-RD, calculated by Dose Reduction Index) for all cell lines treated with combination treatment at IC_{50}.

Combination Index (CI) and Dose Reduction Index (DRI) values were calculated according to Chou Talalay's method (https://doi.org/10.1016/0065-2571(84)90007-4). The CI value <1, =1, and >1 refer to synergistic, additive, and antagonistic effects of the drugs treated in combination, respectively.

B) Level of caspase 3/7 enzyme activity measured after single drug and combination treatment (Reduced Dosed-RD calculated by CompuSyn®, IC_{50} of both the drugs) of 3A.1, DTX and CBZ for 48 h; Combination treatment exhibited higher apoptosis than single drug treatment in mCRPC/NEPC cell lines (PC3, PC3M, DU145, and DUTXR). (* = $p \leq 0.05$). Combination treatment at IC_{50} of both the drugs exhibited the highest level of apoptosis than all other treatments.

C) Gene expression analysis of treated vs. 3A.1 single-agent treated PCa samples showed downregulation of anti-apoptotic genes (BCL2L1, CAPN2, TNFRSF1A, CAPN1, IRAK1, PRKACA, AKT1, NFKBIA, PIK3R2) and upregulation of the pro-apoptotic genes TNFRSF10B, DFFA, RELA, TRADD, and MYD88 (data not shown). This provided additional support that 3A.1 treatment induces apoptosis *in vitro*.

D) Microscope images showing treatment effect on the cell lines PC3, PC3M, DU145, and DUTXR. Results show significantly higher cell death in combination treatment compared to single-drug treatment for all cell lines; ImageJ analysis showed a significant difference in cell density for single

vs combination treatment in cell lines. Results show significantly higher cell death in combination treatment at RD dose compared to single-drug treatment for all the cell lines (* = $p \leq 0.05$).

Figure 3. Differential gene expression profiling of 3A.1 single-agent and combination therapy

A) Heatmaps representing differentially expressed genes (DEGs) following 3A.1 single-agent or combination treatment in human mCRPC/NEPC cell lines (n = 3). Plots represent |fold-change| 1.5 and $p<0.05$ in response to 3A.1, DTX+3A.1 and CBZ+3A.1 treatment, 24 h following drug exposure. Log2 ratios are depicted in a color scale where red represents upregulation and green represents downregulation. I) DEGs for 3A.1 treatment for PCa cell lines. II) DEGs for 3A.1+DTX treatments for PCa cell lines. III) DEGs for 3A.1+DTX treatments for PCa cell lines

Columns represent cell lines, and rows represent genes. Prior to hierarchical clustering, gene expression values were filtered (samples with mean FPKM < 1 or max FPKM < 1 were removed) and z score normalized.

B) Venn diagrams represent unique and common DEGs; based on RNAseq gene expression analysis for 3A.1, DTX+3A.1, CBZ+3A.1 treatment in all cell lines ($p<0.05$).

C) Ingenuity pathway analysis (IPA) predictions; IPA predicted Protein Ubiquitination Pathway (1.73E-19), Unfolded protein response (6.27E-15), NRF2-mediated Oxidative Stress Response (1.96E-11), Aldosterone Signaling in Epithelial Cells (1.08E-10), HIF1α signaling (1.59E-0.05 to 2.29E-0.05), BAG2 Signaling Pathway(1.70E-07), Cell Cycle: G2/M DNA Damage Checkpoint Regulation (1.74E-03), Kinetochore Metaphase Signaling Pathway (5.45E-03), Mitotic Roles of Polo-Like Kinase (2.26E-02) following 3A.1, DTX, CBZ single-agent treatment and as combination treatments. Further, IPA predicted miRNA (miR-21-2) as the top upstream regulator based on the expression of downstream genes.

D) Differential gene expression profiling in acquired resistant mCRPC line DUTXR. I) PCA plots representing show samples clustered based on cell type and treatment. II) Venn diagrams representing unique and common DEGs among various treatment regimens (3A.1 single-agent and combination). III) Graphical summary of IPA analysis for 3A.1 treatment; IV) Pathway comparison analysis between DUTXR vs other mCRPC/NEPC cell lines.

Figure 4. Validation of top DEGs associated with 3A.1 treatment

A) *In Silico* validation: Box plots represent differential MAT2A gene expression among prostate cancer (PRAD) subgroups in the TCGA database. I) MAT2A expression is associated with Gleason score (GS)and II) nodal metastasis status in prostate adenocarcinoma patients (PRAD-TCGA) and III) exhibited post-treatment downregulation of MAT2A expression in our mCRPC/NEPC cell lines.

N0- No regional lymph node metastasis, N1 - Metastases in 1 to 3 axillary lymph nodes.

B) Immunoblotting: Immunoblotting analysis results of proteins representing top DEGs for 3A.1, DTX, CBZ single-agent, and combination treatment in mCRPC/NEPC cell lines. Effect of DTX, CBZ, 3A.1, DTX+3A.1, CBZ+3A.1 treatment on Hsp (70,40,27), MMPs, HIF-1α, and MAT2A levels in mCRPC cell lines were estimated by 24 h treatment followed by protein harvest and immunoblot analysis. B-actin was used as a positive control.

JPET Fast Forward. Published on December 23, 2021 as DOI: 10.1124/jpet.121.000898
This article has not been copyedited and formatted. The final version may differ from this version.

C) Densitometry plots 3A.1, DTX, CBZ dosing-associated (single-agent vs. combination) DEGs compared to Control. Representative protein densitometry analysis: MMP9, MMP-1, MAT2A were significantly downregulated whereas Hsp and HIF-1α were upregulated in 3A.1 single agent and combination treatments with DTX/CBZ compared to control in PCa cell lines.

Figure 5. Functional validation of top IPA-predicted 3A.1 treatment-induced pathways

A) Effect of DTX, CBZ, 3A.1, DTX+3A.1, CBZ+3A.1 treatment on Cell cycle; DUTXR cell was exposed to DTX, CBZ, 3A.1, DTX+3A.1, CBZ+3A.1 treatment for 24 h. Cells were stained with PI, and cell cycle phases were assessed by flow cytometry. Data are presented as the mean ± SEM of three separate experiments (n = 5/study). 3A.1 arrests cell cycle at G1/S checkpoint, in combination treatment (RD, LW-$IC_{50,}$ and IC_{50} of both drugs,) cells are arrested at G1/S more than DTX and CBZ. Cell cycle analysis was performed using CytExpert (Beckman Coulter). Cell Cycle in treatment groups was normalized to corresponding control LW-IC_{50} is the optimal lowest IC_{50} dose of both the drugs among all cell lines. (* = $p \leq 0.05$).

B) COMET assay: Effect 3A.1 treatment on DNA damage (strand breaks) were detected by COMET assay in PC3, PC3M, DU145, and DUTXR cell lines treated with estimated IC_{50} (MTT) for 24 h. A comet appearance is formed with damaged DNA fragments spreading from the center or in the tail. 3A.1 caused DNA damage for all mCRPC cell lines in various degrees. In PC3M (aggressive mCRPC) showed the highest degree of DNA strand breaks by 3A.1 treatment. All images were captured at 4x magnification.

C) Cell migration after 24 and 48 h DTX, CBZ, 3A.1 single agent and in combination (RD, LW-$IC_{50,}$ and IC_{50} of both drugs) 48 h treatments were assessed by measuring Wound healing (Scratch) assay. Combination treatment exhibited reduced wound healing than single-agent treatment mCRPC/NEPC cell line (PC3). RD combination of 3A.1+DTX and 3A.1+CBZ exhibited the highest reduction of cell migration compared to all other treatments. (* = $p \leq 0.05$).

JPET Fast Forward. Published on December 23, 2021 as DOI: 10.1124/jpet.121.000898
This article has not been copyedited and formatted. The final version may differ from this version.

TABLES

Drug	Time (h)	Growth Assay	Mean IC_{50} value			
			PC-3	DU145	PC-3M	DUTXR
3A.1 (µM)	48	MTT	5.74 ± 0.22	3.81 ± 0.03	6.71 ± 0.12	5.45 ± 0.19
		SRB	6.54 ± 0.24	4.07 ± 0.10	5.52 ± 0.25	6.97 ± 0.20
	72	MTT	5.15 ± 0.30	3.62 ± 0.07	4.71 ± 0.10	3.80 ± 0.34
		SRB	4.93 ± 0.32	3.85 ± 0.09	5.29 ± 0.28	4.08 ± 0.06
Docetaxel (nM)	48	MTT	36.8 ± 3.0	13.5 ± 0.8	39.6 ± 3.2	466 ± 17*
		SRB	17.1 ± 2.7	14.5 ± 0.8	6.27 ± 1.11	720 ± 18
Cabazitaxel (nM)	48	MTT	14.5 ± 2.1	6.04 ± 0.45	13.3 ± 2.3	152 ± 11*
		SRB	14.1 ± 0.6	6.51 ± 0.28	11.3 ± 0.1	185 ± 13

Table 1. Effect of single-agent on in vitro cytotoxicity against PCa cell lines

IC_{50} data are presented as mean ± SEM of at least three independent studies (n = 6/study). Values noted with (*) were DUTXR; paclitaxel resistance cell line, showed significantly higher IC_{50} for both DTX and CBZ than other cell lines.

JPET Fast Forward. Published on December 23, 2021 as DOI: 10.1124/jpet.121.000898
This article has not been copyedited and formatted. The final version may differ from this version.

Drug	Cell Line	CI value IC_{50}	DRI value IC_{50}	IC_{50} single agent (nM)	IC_{50} comb with 3A.1 (uM)	CI value IC_{75}	DRI value IC_{75}	IC_{75} single agent (nM)	IC_{75} comb with 3A.1 (nM)	CI value IC_{90}	DRI value IC_{90}	IC_{90} single agent (nM)	IC_{90} comb with 3A.1 (nM)
DTX	PC-3	0.33	4.31	36.76	3.94	0.35	253	366	11.3	0.57	1490	502	32.2
	PC-3M	0.56	4.31	39.63	8.91	0.64	253	658	26.2	1.23	2680	1160	77.5
	DU145	0.48	4.33	13.5	4.17	0.44	10.5	98.7	9.38	0.55	25.6	539	21.1
	DUTXR	0.47	14.0	466	21.9	0.56	19.2	967	50.3	0.68	26.5	3040	116
Drug	**Cell Line**	**CI value IC_{50}**	**DRI value IC_{50}**	**IC_{50} single agent (nM)**	**IC_{50} comb with DTX (uM)**	**CI value IC_{75}**	**DRI value IC_{75}**	**IC_{75} single agent (nM)**	**IC_{75} comb with DTX (nM)**	**CI value IC_{90}**	**DRI value IC_{90}**	**IC_{90} single agent (nM)**	**IC_{90} comb with DTX (nM)**
3A.1	PC-3	0.33	2.98	5.74	0.90	0.35	1.55	7.07	2.26	0.57	0.81	11.4	6.48
	PC-3M	0.56	2.98	6.71	1.78	0.64	1.55	8.17	5.25	1.23	1.06	12.6	15.5
	DU145	0.48	3.95	3.81	0.83	0.44	2.91	5.46	1.87	0.55	2.14	9.02	4.21
	DUTXR	0.47	2.46	6.97	2.18	0.56	1.56	9.85	5.02	0.68	1.56	18.1	11.6
Drug	**Cell Line**	**CI value IC_{50}**	**DRI value IC_{50}**	**IC_{50} single agent (nM)**	**IC_{50} comb with 3A.1 (nM)**	**CI value IC_{75}**	**DRI value IC_{75}**	**IC_{75} single agent (nM)**	**IC_{75} comb with 3A.1 (nM)**	**CI value IC_{90}**	**DRI value IC_{90}**	**IC_{90} single agent (nM)**	**IC_{90} comb with 3A.1 (nM)**
CBZ	PC-3	0.51	1.83	14.5	4.0	0.76	27.0	46.5	6.34	0.90	397	399	11.28
	PC-3M	0.79	1.83	13.3	6.66	0.49	27.0	204	18.7	0.83	397	2080	52.53
	DU145	0.6	2.51	6.04	3.45	0.43	7.22	57.1	7.91	0.45	20.8	338	18.13
	DUTXR	0.26	14.4	152	10.3	0.38	46.3	1680	36.2	0.70	149	18854	126.6
Drug	**Cell Line**	**CI value IC_{50}**	**DRI value IC_{50}**	**IC_{50} single agent (nM)**	**IC_{50} comb with CBZ (uM)**	**CI value IC_{75}**	**DRI value IC_{75}**	**IC_{75} single agent (nM)**	**IC_{75} comb with CBZ (nM)**	**CI value IC_{90}**	**DRI value IC_{90}**	**IC_{90} single agent (nM)**	**IC_{90} comb with CBZ (nM)**
3A.1	PC-3	0.51	3.98	5.74	1.9	0.76	2.18	6.04	1.01	0.9	1.2	11.4	10.1
	PC-3M	0.79	3.98	6.71	1.3	0.49	2.18	8.17	3.73	0.83	1.2	12.6	10.5
	DU145	0.6	4.79	3.81	0.7	0.43	3.45	5.45	1.59	0.45	2.49	9.02	3.62
	DUTXR	0.26	5.19	6.97	1.03	0.38	2.72	9.85	3.62	0.7	1.43	18.1	12.7

Table 2. Effect of Combination (DTX+3A.1 and CBZ+3A.1) treatments on in vitro cytotoxicity against PCa cell lines

To evaluate the pharmacological interactions, % of cells were affected (fraction affected - Fa) by DTX or CBZ, and 3A.1 treatment was analyzed by CompuSyn® version 1.0 software. The combination index (CI) value was calculated according to Chou's method (https://doi.org/10.1016/0065-2571(84)90007-4).

JPET Fast Forward. Published on December 23, 2021 as DOI: 10.1124/jpet.121.000898
This article has not been copyedited and formatted. The final version may differ from this version.

The CI value <1, =1, and >1 refer to the synergistic, additive, and antagonistic effects of the drugs treated in combination, respectively. Dose reduction index (DRI) was calculated for each drug combination of all cell lines, where DRI > 1 indicates that drug combination reduces the dose of a specific drug compared with the dose of the same drug as single-drug treatment.

JPET Fast Forward. Published on December 23, 2021 as DOI: 10.1124/jpet.121.000898
This article has not been copyedited and formatted. The final version may differ from this version.

Gene Symbol	Fold change log (3A.1 vs. No treatment)	P-value (3A.1 vs. No treatment)	Fold change log (Doce+3A.1 vs. No treatment)	P-value (DTX+3A.1 vs. No treatment)	Fold change log (CBZ+3A.1 vs. No treatment)	P-value (CBZ+3A.1 vs. No treatment)
HSPA6/ Hsp70B	8.39	1.78E-06	8.47	1.89E-06	8.16	2.09E-06
ARC	7.31	7.32E-05	7.57	1.10E-04	7.35	3.66E-05
HSPA1B/ Hsp70-2	7.00	8.99E-08	6.91	9.76E-08	6.88	1.43E-06
HSPA1A/HsP70-1	6.98	1.41E-07	6.90	1.58E-07	6.88	9.89E-08
HMOX1	6.54	2.13E-06	6.56	1.88E-06	6.88	1.51E-07
DNAJB1/Hsp40	5.55	7.49E-06	5.37	9.65E-06	5.64	6.43E-06
RPPH1	4.94	8.38E-03	NA	NA	NA	NA
BAG3	4.89	7.56E-06	4.75	8.88E-06	5.15	5.39E-06
HSPB1/Hsp27	4.67	6.39E-06	4.55	7.57E-06	4.53	6.80E-04
HSPH1/Hsp110	4.62	7.64E-04	4.40	9.52E-04	4.85	3.70E-06
ZFAND2A	4.39	8.01E-06	4.46	5.26E-05	4.75	7.59E-06
GABARAPL1	3.79	5.87E-05	3.80	5.26E-05	4.51	1.91E-05
OTUD1	3.66	3.08E-04	3.45	3.95E-04	3.65	1.64E-06
ADM	3.55	2.86E-02	3.60	3.35E-02	3.81	2.99E-05
UBC	3.54	4.41E-06	3.41	5.78E-06	3.48	1.80E-02
CXCL8	3.51	3.82E-02	3.20	4.52E-02	3.45	1.07E-04
DUSP1	NA	NA	NA	NA	3.49	5.01E-04
DDIT3	NA	NA	NA	NA	3.47	9.20E-04
HSP90AA1/Hsp90	3.46	1.01E-04	3.35	1.13E-04	3.73	8.27E-05
PPP1R15A	3.43	1.60E-04	3.55	1.08E-04	4.07	3.18E-02
DDIT4	3.36	1.06E-05	3.54	6.50E-06	4.26	5.03E-04
DEDD2	3.33	1.71E-06	3.34	1.87E-06	3.55	6.68E-07
SAT1	3.29	4.38E-04	3.50	2.93E-04	3.78	2.88E-04
ANXA1	3.29	2.67E-04	3.08	4.26E-04	3.54	1.05E-02
MMP1	3.28	1.17E-02	3.31	1.17E-02	3.52	1.05E-02
SESN2	3.16	1.10E-06	3.06	1.71E-06	NA	NA
UBB	3.09	1.51E-02	3.23	1.28E-02	NA	NA
CDKN1A	NA	NA	3.05	3.63E-03	NA	NA
SELENON	NA	NA	-1.40	3.32E-03	NA	NA
FAM210B	NA	NA	-1.42	7.19E-03	NA	NA
SLC25A23	NA	NA	-1.43	4.80E-02	NA	NA
SPATA20	NA	NA	-1.43	3.01E-03	NA	NA
CD3EAP	NA	NA	-1.47	1.41E-03	-1.67	3.94E-04
MYADM	NA	NA	-1.58	1.10E-02	-1.08	3.37E-02
MXD3	NA	NA	NA	NA	-1.22	1.02E-02
CISD3	-1.57	3.06E-03	-1.43	5.77E-03	NA	NA

JPET Fast Forward. Published on December 23, 2021 as DOI: 10.1124/jpet.121.000898
This article has not been copyedited and formatted. The final version may differ from this version.

ABHD14B	NA	NA	-1.60	4.11E-02	NA	NA
PIGW	NA	NA	-1.61	4.41E-03	-1.34	1.25E-02
TMEM129	-1.62	5.92E-04	-1.67	6.76E-04	NA	NA
SRM	-1.62	2.98E-02	-1.54	2.49E-02	NA	NA
GAS2L1	-1.63	3.21E-02	NA	NA	NA	NA
DHCR7	NA	NA	-1.63	1.51E-02	NA	NA
ICAM3	-1.65	4.65E-02	NA	NA	NA	NA
IGFBP4	NA	NA	-1.65	1.25E-03	-1.37	4.96E-03
GM2A	NA	NA	-1.69	1.98E-03	NA	NA
PARD6A	NA	NA	-1.71	1.56E-03	-1.23	1.36E-02
PIGM	-1.71	6.56E-03	-1.70	8.94E-03	-1.36	3.16E-02
PAQR4	-1.72	6.06E-03	-1.86	4.77E-03	-1.35	4.25E-02
THEM6	-1.72	4.96E-02	-1.89	2.45E-02	NA	NA
HYAL2	-1.75	1.93E-03	-1.72	2.39E-03	NA	NA
ATP6V0E2	-1.78	4.96E-03	-1.82	1.03E-02	NA	NA
NDUFB1	-1.82	1.96E-02	NA	NA	NA	NA
SAPCD2	-1.87	6.87E-03	NA	NA	NA	NA
RBM3	-1.88	7.13E-04	-1.70	1.63E-03	-1.36	4.99E-03
MARS2	NA	NA	-1.93	4.11E-02	NA	NA
GGCX	-2.05	1.20E-02	-1.67	4.58E-02	NA	NA
PSRC1	-2.18	1.65E-02	NA	NA	NA	NA
PCNA-AS1	-2.24	1.67E-02	NA	NA	-1.80	2.76E-02
MAT2A	-2.62	3.09E-03	-2.58	3.63E-03	-2.49	5.11E-03
MTRNR2L2	NA	NA	NA	NA	NA	9.16E-03

Table 3 Top differentially expressed genes (DEGs)

Fold change compared to the untreated group for each cell line. Following 48 h of 3A.1, 3A.1+DTX and 3A.1+CBZ treatment in PC-3, PC-3M, DU145 (AI-mCRPC/NEPC) cell lines. Fold change cut-off value is >1.5. Hsp70, Hsp40, Hsp27, Hsp110, ARC, HMOX1, and BAG3 were expressed (upregulated) in all treatment groups, but there was variation in expression levels. MAT2A, RBM3, PAQR4, and PIGM these genes were downregulated in all treatment groups.

Figure 1.

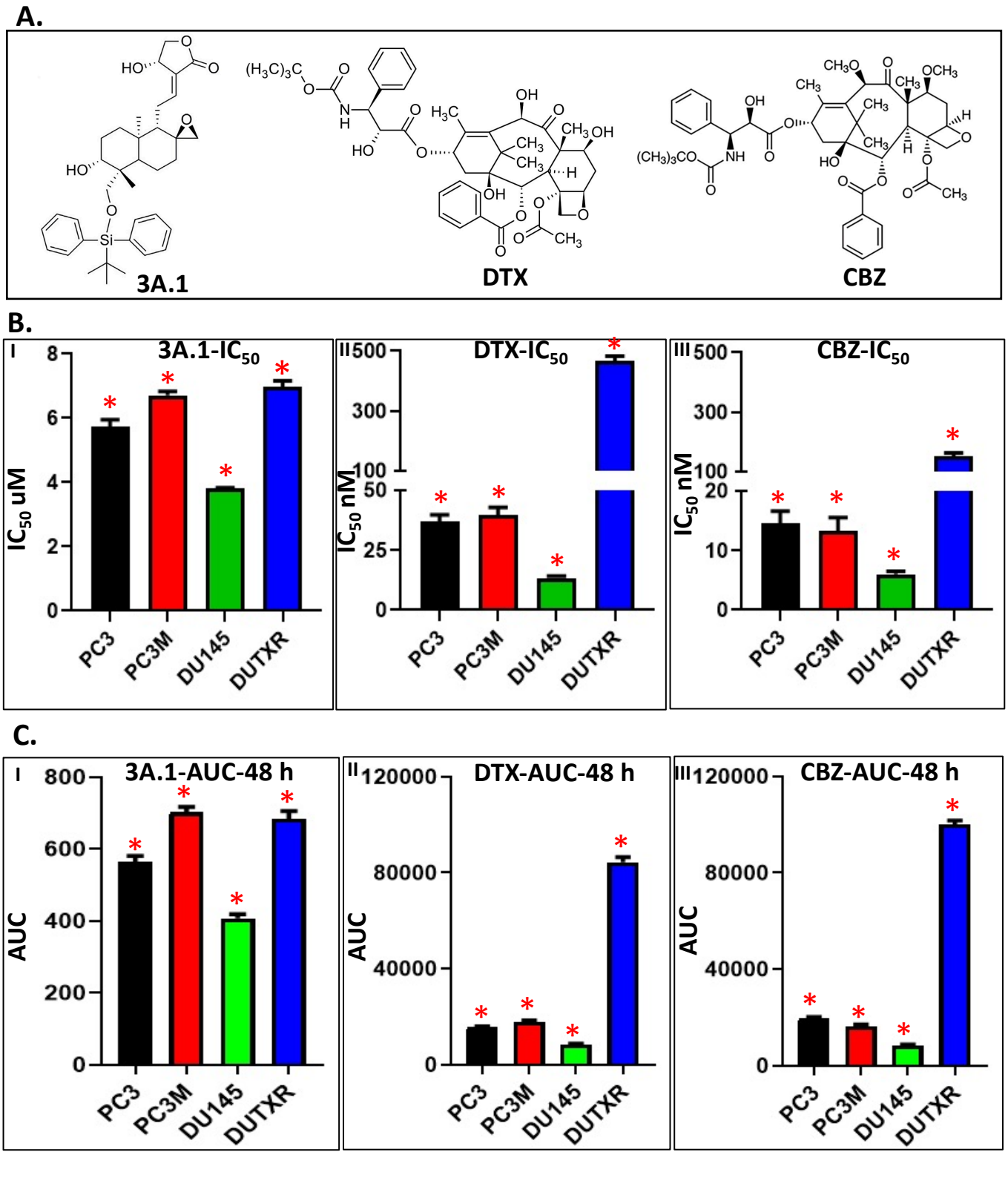
A.
3A.1
DTX
CBZ
B.
I
3A.1-IC50
IC50 uM
II
DTX-IC50
IC50 nM
III
CBZ-IC50
IC50 nM
PC3
PC3M
DU145
DUTXR
C.
I
3A.1-AUC-48 h
AUC
II
DTX-AUC-48 h
AUC
III
CBZ-AUC-48 h
AUC

Figure 2.

A.

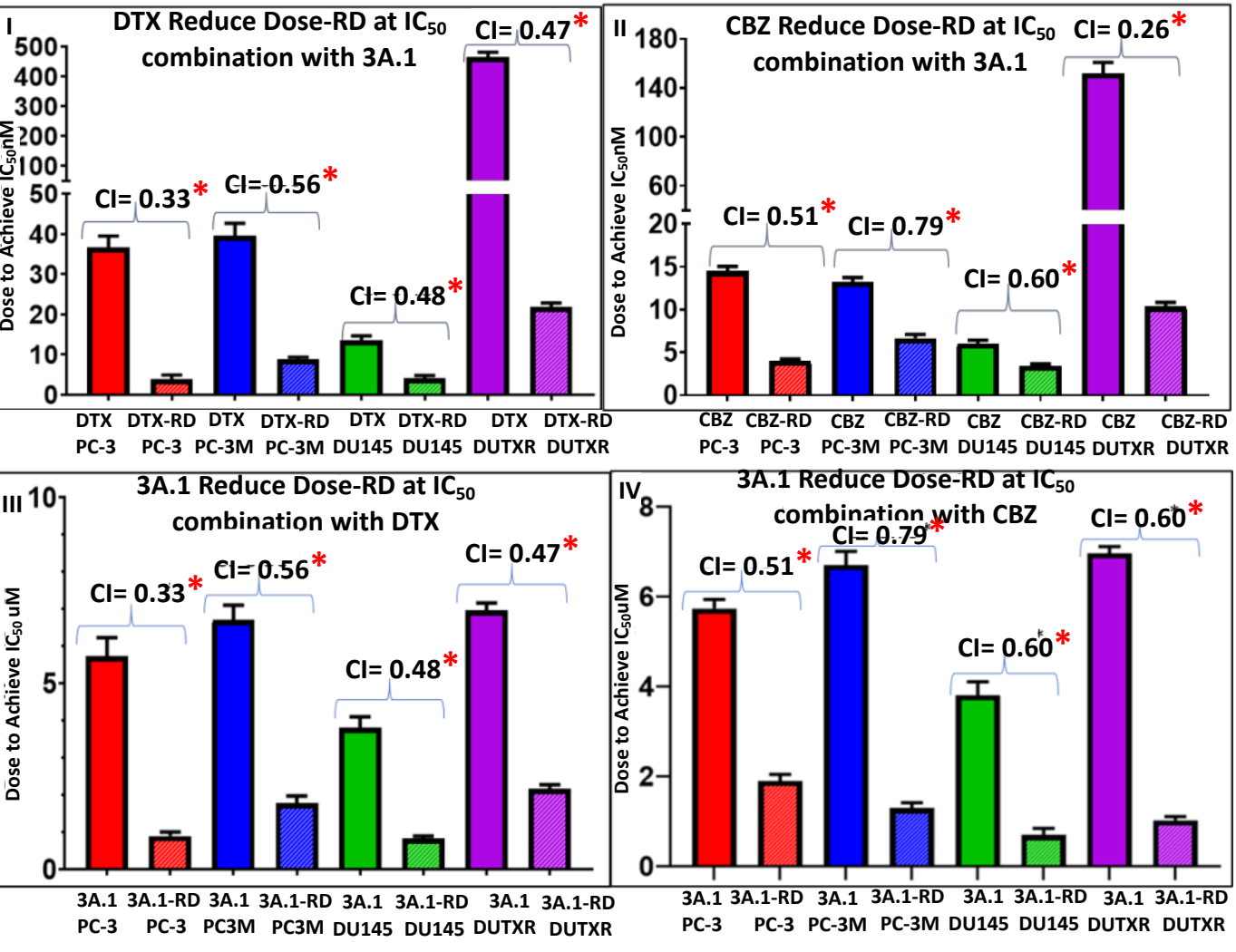
I
DTX Reduce Dose-RD at IC50
combination with 3A.1
Dose to Achieve IC50nM
CI= 0.33*
CI= 0.56*
CI= 0.48*
CI= 0.47*
DTX PC-3
DTX-RD PC-3
DTX PC-3M
DTX-RD PC-3M
DTX DU145
DTX-RD DU145
DTX DUTXR
DTX-RD DUTXR
II
CBZ Reduce Dose-RD at IC50
combination with 3A.1
Dose to Achieve IC50nM
CI= 0.51*
CI= 0.79*
CI= 0.60*
CI= 0.26*
CBZ PC-3
CBZ-RD PC-3
CBZ PC-3M
CBZ-RD PC-3M
CBZ DU145
CBZ-RD DU145
CBZ DUTXR
CBZ-RD DUTXR
III
3A.1 Reduce Dose-RD at IC50
combination with DTX
Dose to Achieve IC50 uM
CI= 0.33*
CI= 0.56*
CI= 0.48*
CI= 0.47*
3A.1 PC-3
3A.1-RD PC-3
3A.1 PC3M
3A.1-RD PC3M
3A.1 DU145
3A.1-RD DU145
3A.1 DUTXR
3A.1-RD DUTXR
IV
3A.1 Reduce Dose-RD at IC50
combination with CBZ
Dose to Achieve IC50uM
CI= 0.51*
CI= 0.79*
CI= 0.60*
CI= 0.60*
3A.1 PC-3
3A.1-RD PC-3
3A.1 PC-3M
3A.1-RD PC-3M
3A.1 DU145
3A.1-RD DU145
3A.1 DUTXR
3A.1-RD DUTXR

Figure 2.

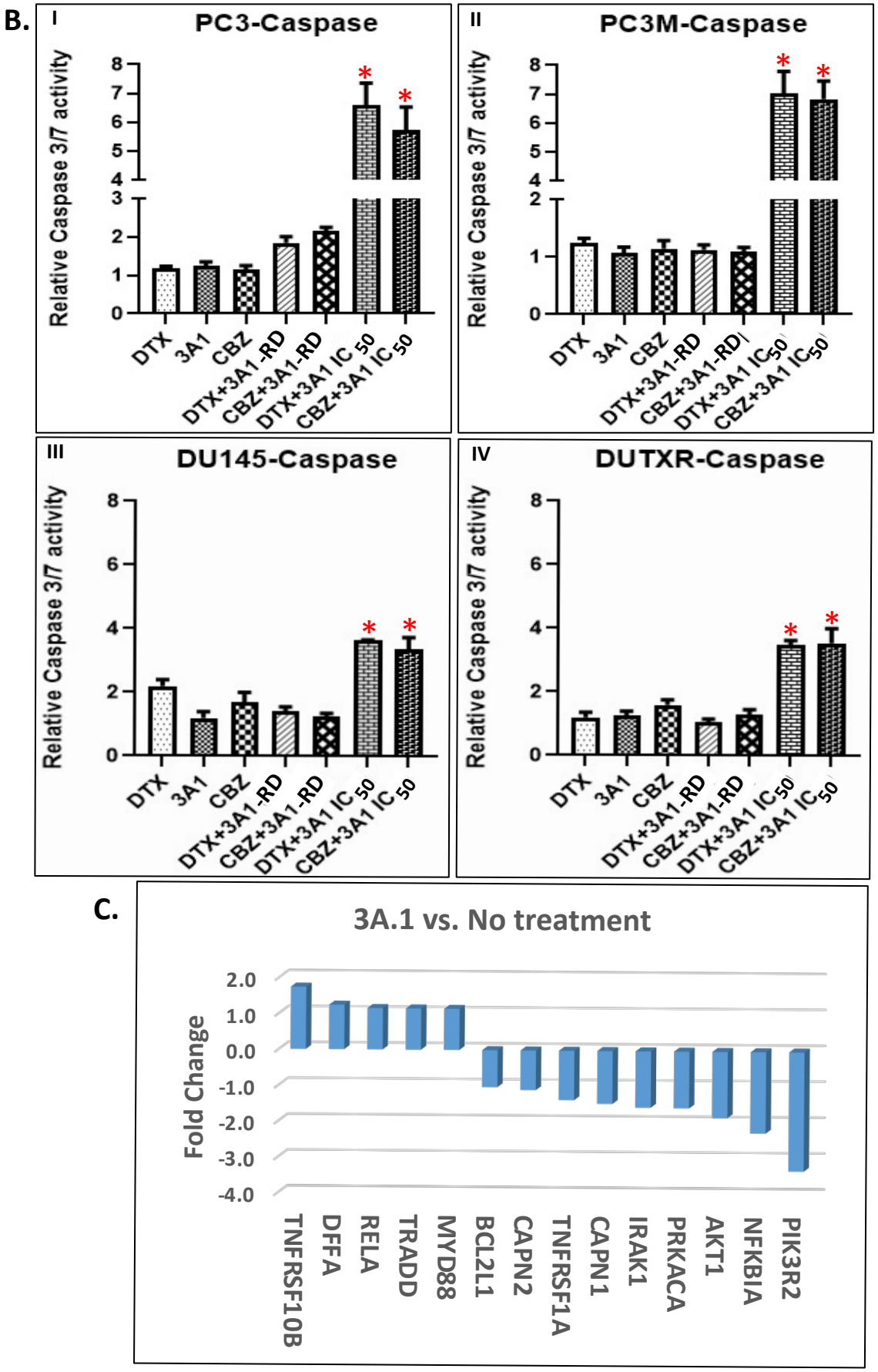
B.
I
PC3-Caspase
Relative Caspase 3/7 activity
DTX
3A1
CBZ
DTX+3A1-RD
CBZ+3A1-RD
DTX+3A1 IC50
CBZ+3A1 IC50
II
PC3M-Caspase
III
DU145-Caspase
IV
DUTXR-Caspase
C.
3A.1 vs. No treatment
Fold Change
TNFRSF10B
DFFA
RELA
TRADD
MYD88
BCL2L1
CAPN2
TNFRSF1A
CAPN1
IRAK1
PRKACA
AKT1
NFKBIA
PIK3R2

Figure 2.

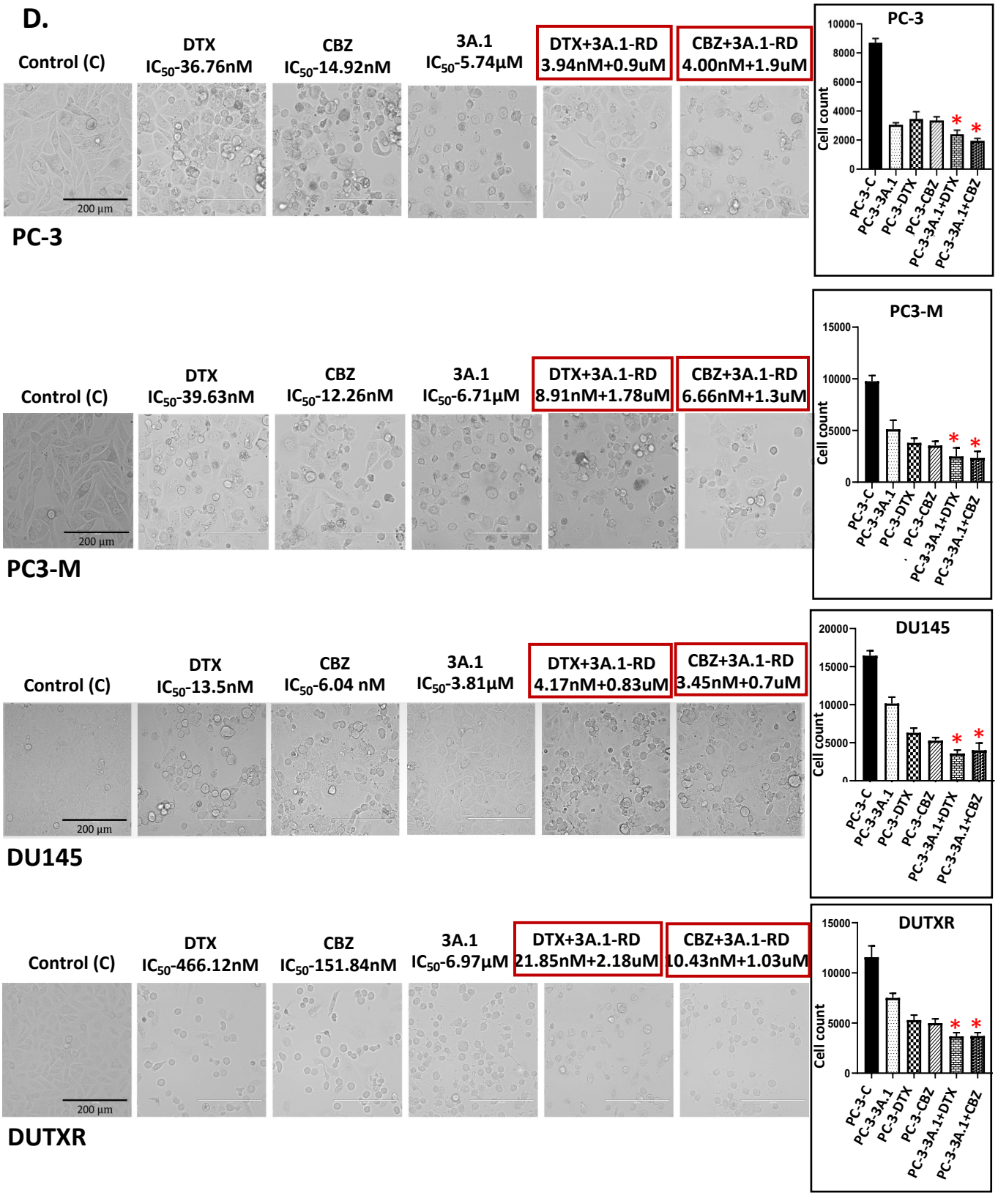
D.
Control (C)
DTX
IC50-36.76nM
CBZ
IC50-14.92nM
3A.1
IC50-5.74μM
DTX+3A.1-RD
3.94nM+0.9uM
CBZ+3A.1-RD
4.00nM+1.9uM
200 μm
PC-3
PC-3
Cell count
PC-3-C
PC-3-3A.1
PC-3-DTX
PC-3-CBZ
PC-3-3A.1+DTX
PC-3-3A.1+CBZ
Control (C)
DTX
IC50-39.63nM
CBZ
IC50-12.26nM
3A.1
IC50-6.71μM
DTX+3A.1-RD
8.91nM+1.78uM
CBZ+3A.1-RD
6.66nM+1.3uM
200 μm
PC3-M
PC3-M
Cell count
Control (C)
DTX
IC50-13.5nM
CBZ
IC50-6.04 nM
3A.1
IC50-3.81μM
DTX+3A.1-RD
4.17nM+0.83uM
CBZ+3A.1-RD
3.45nM+0.7uM
200 μm
DU145
DU145
Cell count
Control (C)
DTX
IC50-466.12nM
CBZ
IC50-151.84nM
3A.1
IC50-6.97μM
DTX+3A.1-RD
21.85nM+2.18uM
CBZ+3A.1-RD
10.43nM+1.03uM
200 μm
DUTXR
DUTXR
Cell count

Figure 3.

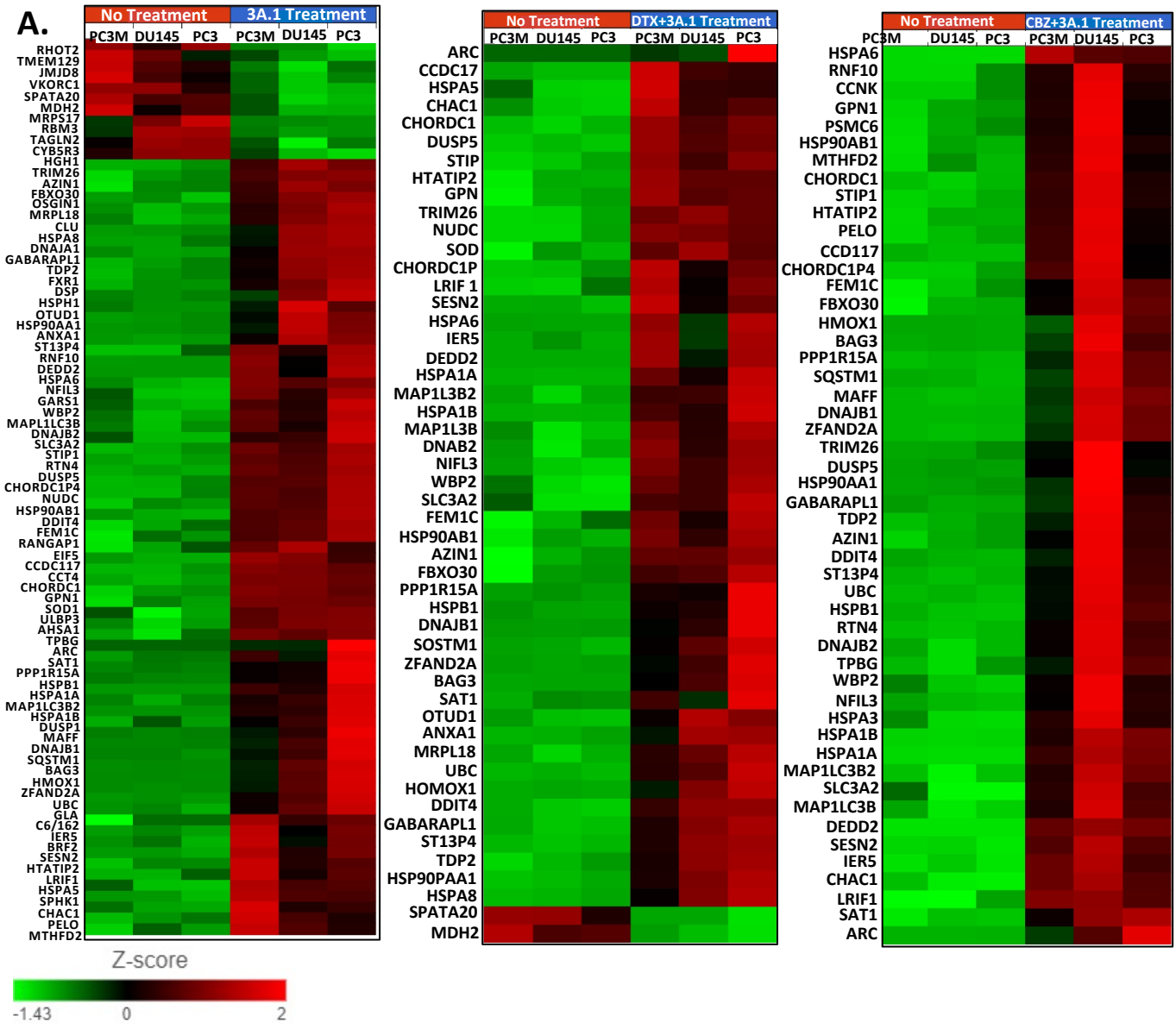
A.
No Treatment
3A.1 Treatment
PC3M DU145 PC3 PC3M DU145 PC3
RHOT2
TMEM129
JMJD8
VKORC1
SPATA20
MDH2
MRPS17
RBM3
TAGLN2
CYB5R3
HGH1
TRIM26
AZIN1
FBXO30
OSGIN1
MRPL18
CLU
HSPA8
DNAJA1
GABARAPL1
TDP2
FXR1
DSP
HSPH1
OTUD1
HSP90AA1
ANXA1
ST13P4
RNF10
DEDD2
HSPA6
NFIL3
GARS1
WBP2
MAPL1LC3B
DNAJB2
SLC3A2
STIP1
RTN4
DUSP5
CHORDC1P4
NUDC
HSP90AB1
DDIT4
FEM1C
RANGAP1
EIF5
CCDC117
CCT4
CHORDC1
GPN1
SOD1
ULBP3
AHSA1
TPBG
ARC
SAT1
PPP1R15A
HSPB1
HSPA1A
MAP1LC3B2
HSPA1B
DUSP1
MAFF
DNAJB1
SQSTM1
BAG3
HMOX1
ZFAND2A
UBC
GLA
C6/162
IER5
BRF2
SESN2
HTATIP2
LRIF1
HSPA5
SPHK1
CHAC1
PELO
MTHFD2
No Treatment
DTX+3A.1 Treatment
PC3M DU145 PC3 PC3M DU145 PC3
ARC
CCDC17
HSPA5
CHAC1
CHORDC1
DUSP5
STIP
HTATIP2
GPN
TRIM26
NUDC
SOD
CHORDC1P
LRIF 1
SESN2
HSPA6
IER5
DEDD2
HSPA1A
MAP1L3B2
HSPA1B
MAP1L3B
DNAB2
NIFL3
WBP2
SLC3A2
FEM1C
HSP90AB1
AZIN1
FBXO30
PPP1R15A
HSPB1
DNAJB1
SOSTM1
ZFAND2A
BAG3
SAT1
OTUD1
ANXA1
MRPL18
UBC
HOMOX1
DDIT4
GABARAPL1
ST13P4
TDP2
HSP90PAA1
HSPA8
SPATA20
MDH2
No Treatment
CBZ+3A.1 Treatment
PC3M DU145 PC3 PC3M DU145 PC3
HSPA6
RNF10
CCNK
GPN1
PSMC6
HSP90AB1
MTHFD2
CHORDC1
STIP1
HTATIP2
PELO
CCD117
CHORDC1P4
FEM1C
FBXO30
HMOX1
BAG3
PPP1R15A
SQSTM1
MAFF
DNAJB1
ZFAND2A
TRIM26
DUSP5
HSP90AA1
GABARAPL1
TDP2
AZIN1
DDIT4
ST13P4
UBC
HSPB1
RTN4
DNAJB2
TPBG
WBP2
NFIL3
HSPA3
HSPA1B
HSPA1A
MAP1LC3B2
SLC3A2
MAP1LC3B
DEDD2
SESN2
IER5
CHAC1
LRIF1
SAT1
ARC
Z-score
-1.43
0
2

B.

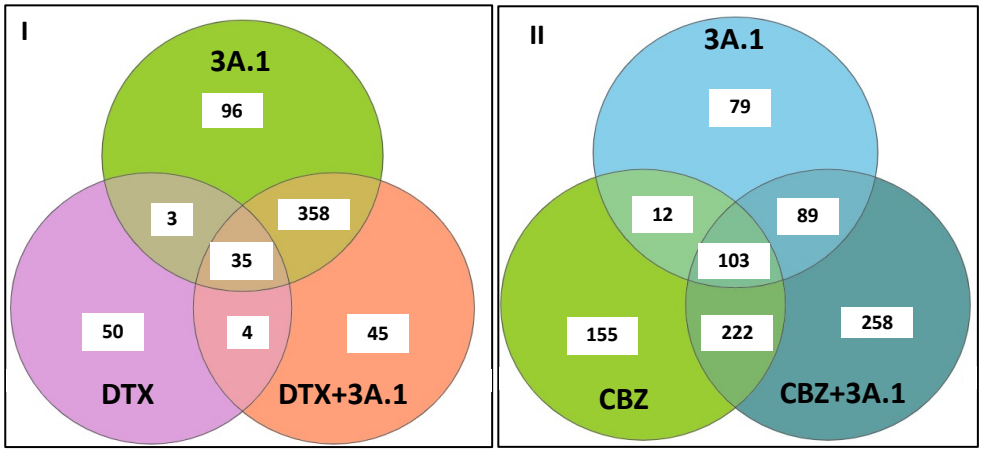
I
3A.1
96
3
358
35
50
4
45
DTX
DTX+3A.1
II
3A.1
79
12
89
103
155
222
258
CBZ
CBZ+3A.1

Figure 3.

C.

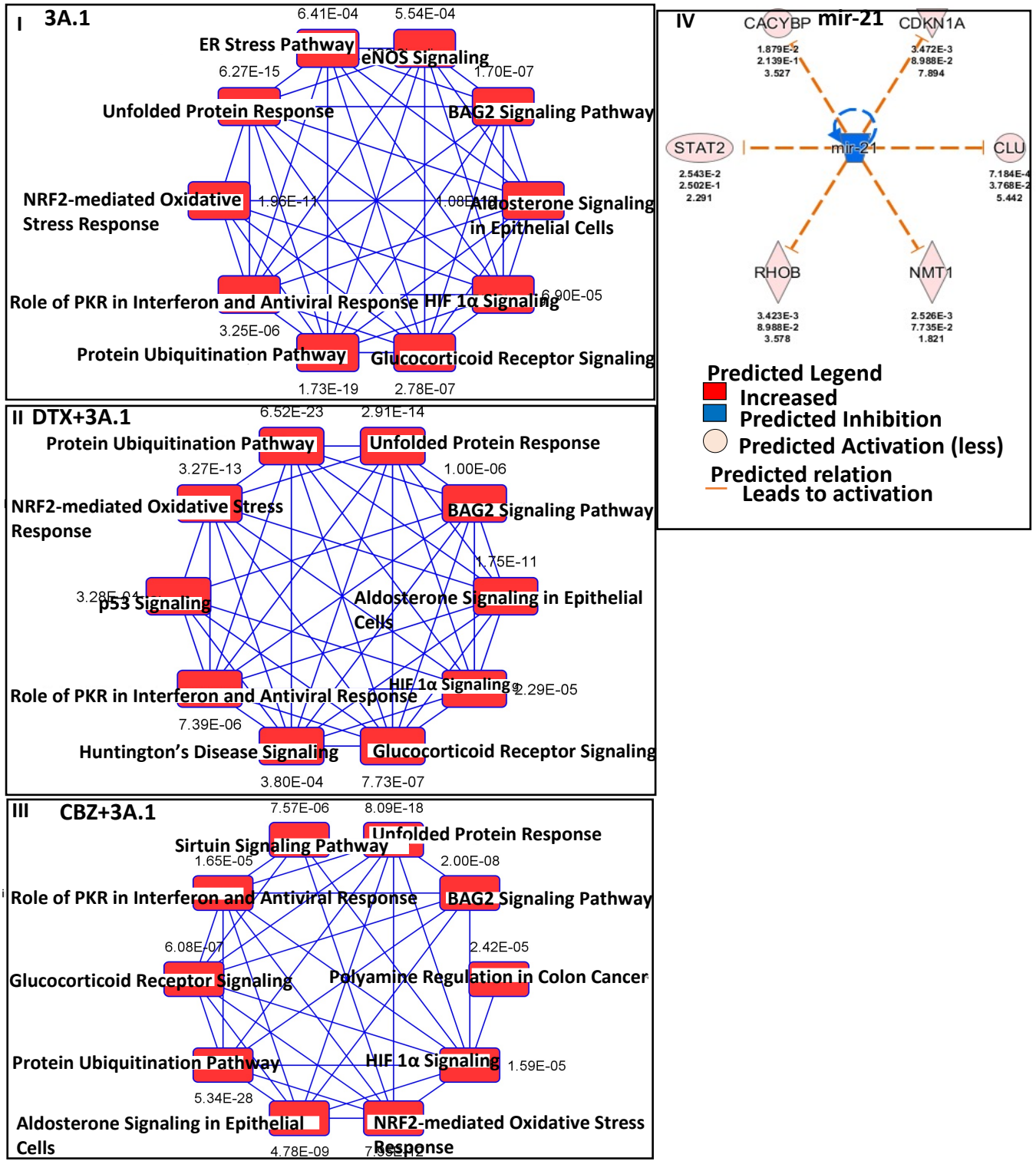
I 3A.1
6.41E-04
5.54E-04
ER Stress Pathway
eNOS Signaling
6.27E-15
1.70E-07
Unfolded Protein Response
BAG2 Signaling Pathway
NRF2-mediated Oxidative Stress Response
1.96E-11
1.08E-11
Aldosterone Signaling in Epithelial Cells
Role of PKR in Interferon and Antiviral Response
HIF 1α Signaling
6.90E-05
3.25E-06
Protein Ubiquitination Pathway
Glucocorticoid Receptor Signaling
1.73E-19
2.78E-07
II DTX+3A.1
6.52E-23
2.91E-14
Protein Ubiquitination Pathway
Unfolded Protein Response
3.27E-13
1.00E-06
NRF2-mediated Oxidative Stress Response
BAG2 Signaling Pathway
1.75E-11
p53 Signaling
Aldosterone Signaling in Epithelial Cells
Role of PKR in Interferon and Antiviral Response
HIF 1α Signaling
2.29E-05
7.39E-06
Huntington's Disease Signaling
Glucocorticoid Receptor Signaling
3.80E-04
7.73E-07
III CBZ+3A.1
7.57E-06
8.09E-18
Sirtuin Signaling Pathway
Unfolded Protein Response
1.65E-05
2.00E-08
Role of PKR in Interferon and Antiviral Response
BAG2 Signaling Pathway
6.08E-07
2.42E-05
Glucocorticoid Receptor Signaling
Polyamine Regulation in Colon Cancer
Protein Ubiquitination Pathway
HIF 1α Signaling
1.59E-05
5.34E-28
Aldosterone Signaling in Epithelial Cells
NRF2-mediated Oxidative Stress Response
4.78E-09
IV
CACYBP
mir-21
CDKN1A
1.879E-2
2.139E-1
3.527
3.472E-3
8.988E-2
7.894
STAT2
mir-21
CLU
2.543E-2
2.502E-1
2.291
7.184E-4
3.768E-2
5.442
RHOB
NMT1
3.423E-3
8.988E-2
3.578
2.526E-3
7.735E-2
1.821
Predicted Legend
Increased
Predicted Inhibition
Predicted Activation (less)
Predicted relation
Leads to activation

Figure 3.

D.

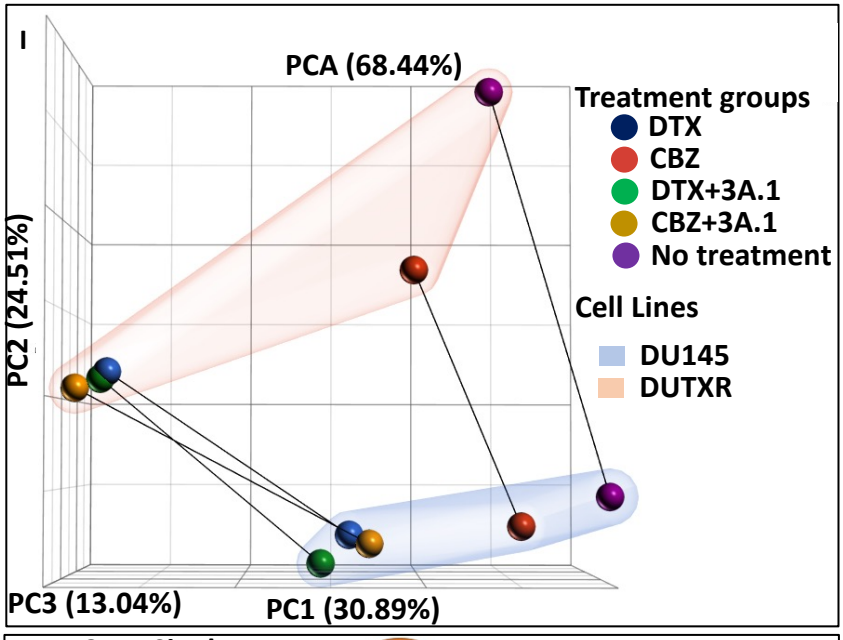
I
PCA (68.44%)
PC2 (24.51%)
PC3 (13.04%)
PC1 (30.89%)
Treatment groups
DTX
CBZ
DTX+3A.1
CBZ+3A.1
No treatment
Cell Lines
DU145
DUTXR

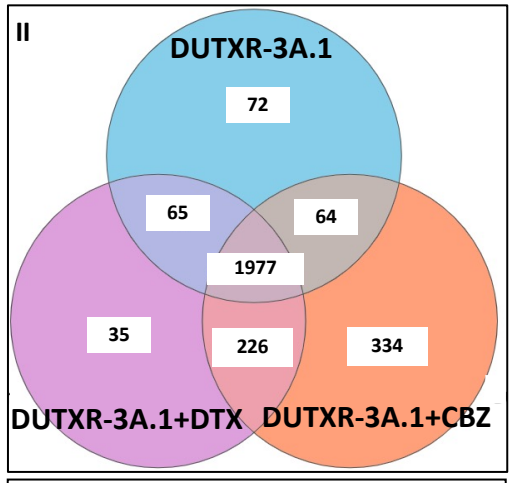
II
DUTXR-3A.1
72
65
64
1977
35
226
334
DUTXR-3A.1+DTX
DUTXR-3A.1+CBZ

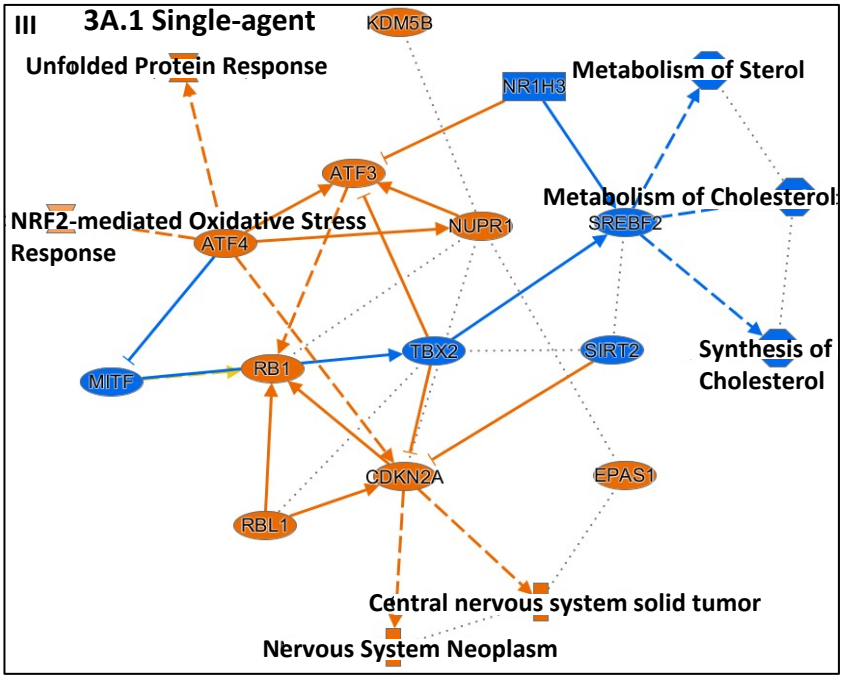
III
3A.1 Single-agent
KDM5B
Unfolded Protein Response
NR1H3
Metabolism of Sterol
ATF3
Metabolism of Cholesterol
NRF2-mediated Oxidative Stress Response
ATF4
NUPR1
SREBF2
MITF
RB1
TBX2
SIRT2
Synthesis of Cholesterol
CDKN2A
EPAS1
RBL1
Central nervous system solid tumor
Nervous System Neoplasm

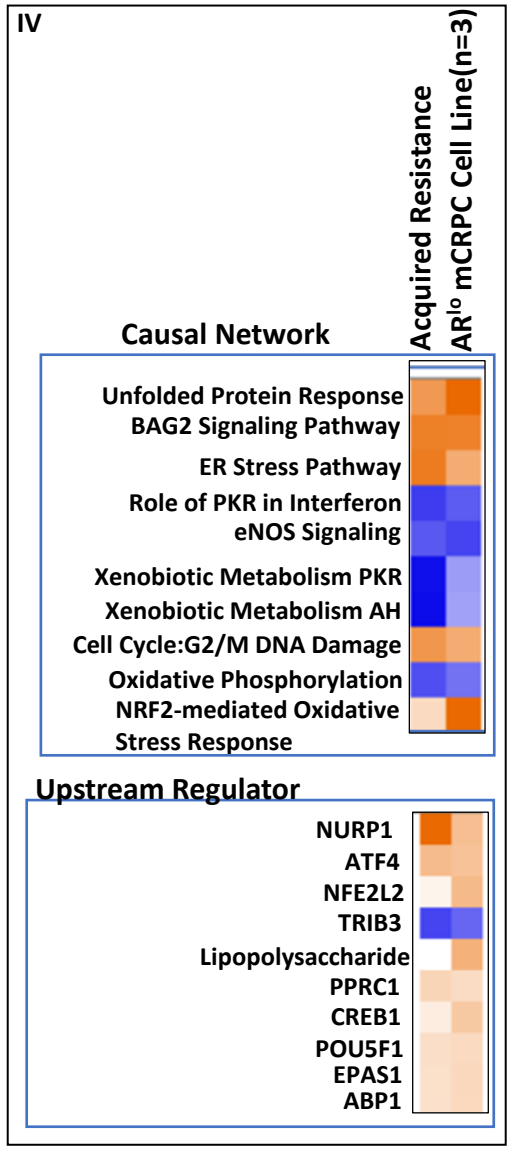
IV
Acquired Resistance
ARlo mCRPC Cell Line(n=3)
Causal Network
Unfolded Protein Response
BAG2 Signaling Pathway
ER Stress Pathway
Role of PKR in Interferon
eNOS Signaling
Xenobiotic Metabolism PKR
Xenobiotic Metabolism AH
Cell Cycle:G2/M DNA Damage
Oxidative Phosphorylation
NRF2-mediated Oxidative
Stress Response
Upstream Regulator
NURP1
ATF4
NFE2L2
TRIB3
Lipopolysaccharide
PPRC1
CREB1
POU5F1
EPAS1
ABP1

Figure 4.

A.

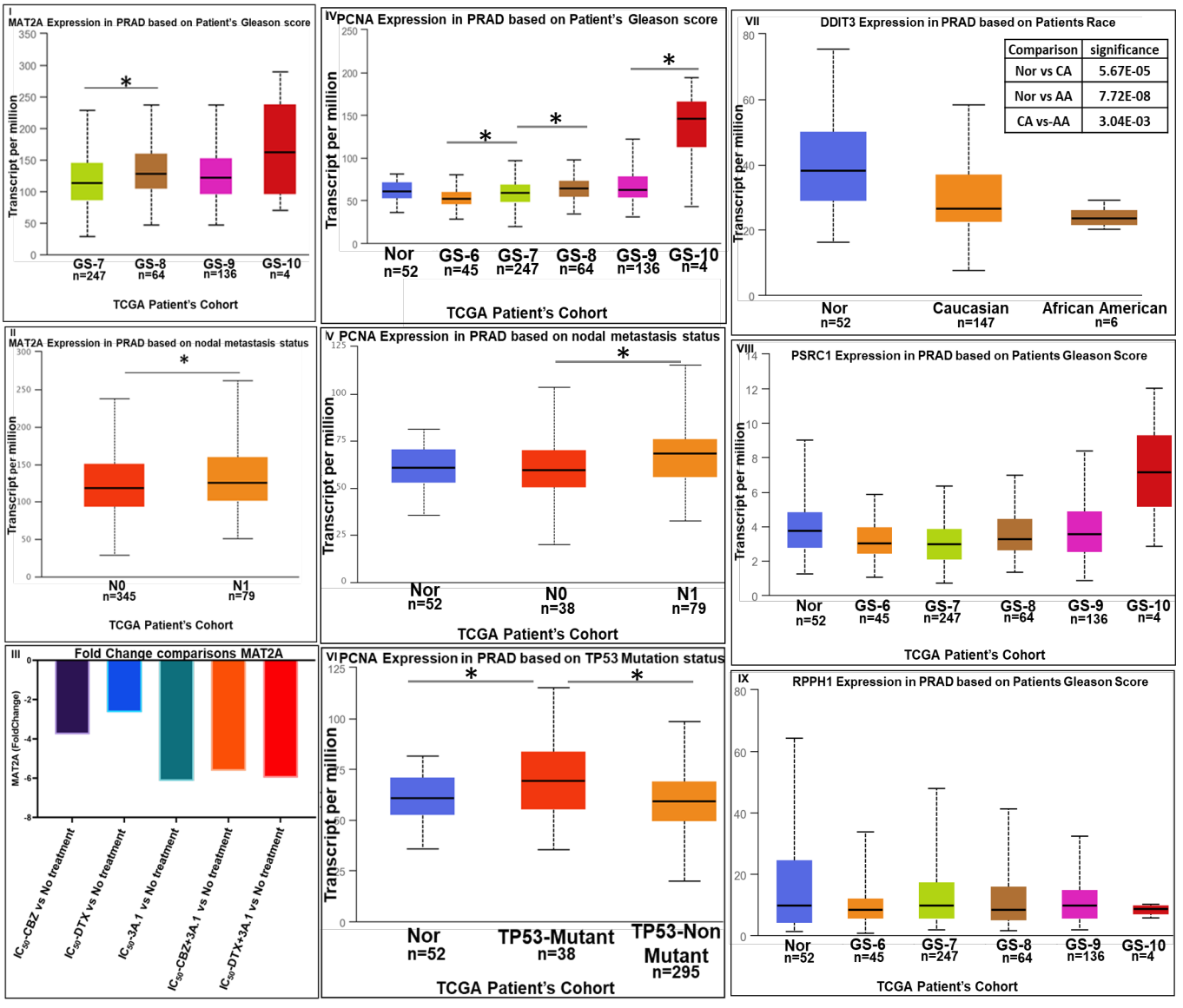
I
MAT2A Expression in PRAD based on Patient's Gleason score
Transcript per million
GS-7 n=247
GS-8 n=64
GS-9 n=136
GS-10 n=4
TCGA Patient's Cohort
II
MAT2A Expression in PRAD based on nodal metastasis status
Transcript per million
N0 n=345
N1 n=79
TCGA Patient's Cohort
III
Fold Change comparisons MAT2A
MAT2A (FoldChange)
IC50-CBZ vs No treatment
IC50-DTX vs No treatment
IC50-3A.1 vs No treatment
IC50-CBZ+3A.1 vs No treatment
IC50-DTX+3A.1 vs No treatment
IV
PCNA Expression in PRAD based on Patient's Gleason score
Transcript per million
Nor n=52
GS-6 n=45
GS-7 n=247
GS-8 n=64
GS-9 n=136
GS-10 n=4
TCGA Patient's Cohort
V
PCNA Expression in PRAD based on nodal metastasis status
Transcript per million
Nor n=52
N0 n=38
N1 n=79
TCGA Patient's Cohort
VI
PCNA Expression in PRAD based on TP53 Mutation status
Transcript per million
Nor n=52
TP53-Mutant n=38
TP53-Non Mutant n=295
TCGA Patient's Cohort
VII
DDIT3 Expression in PRAD based on Patients Race
Comparison | significance
Nor vs CA | 5.67E-05
Nor vs AA | 7.72E-08
CA vs-AA | 3.04E-03
Transcript per million
Nor n=52
Caucasian n=147
African American n=6
VIII
PSRC1 Expression in PRAD based on Patients Gleason Score
Transcript per million
Nor n=52
GS-6 n=45
GS-7 n=247
GS-8 n=64
GS-9 n=136
GS-10 n=4
TCGA Patient's Cohort
IX
RPPH1 Expression in PRAD based on Patients Gleason Score
Nor n=52
GS-6 n=45
GS-7 n=247
GS-8 n=64
GS-9 n=136
GS-10 n=4
TCGA Patient's Cohort

Figure 4.

B.

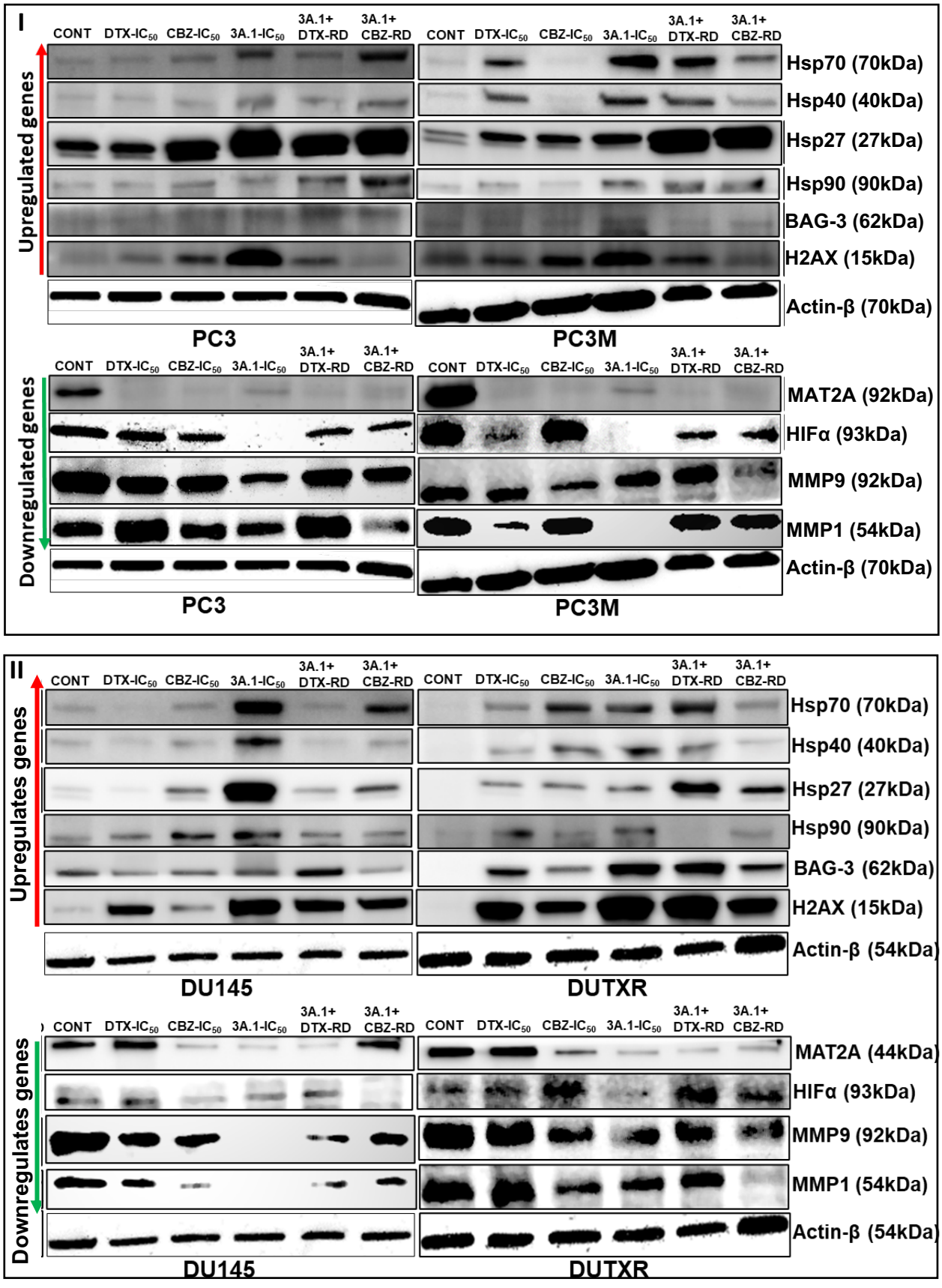
I
CONT
DTX-IC50
CBZ-IC50
3A.1-IC50
3A.1+ DTX-RD
3A.1+ CBZ-RD
Upregulated genes
Hsp70 (70kDa)
Hsp40 (40kDa)
Hsp27 (27kDa)
Hsp90 (90kDa)
BAG-3 (62kDa)
H2AX (15kDa)
Actin-β (70kDa)
PC3
PC3M
Downregulated genes
MAT2A (92kDa)
HIFα (93kDa)
MMP9 (92kDa)
MMP1 (54kDa)
Actin-β (70kDa)
II
Upregulates genes
Hsp70 (70kDa)
Hsp40 (40kDa)
Hsp27 (27kDa)
Hsp90 (90kDa)
BAG-3 (62kDa)
H2AX (15kDa)
Actin-β (54kDa)
DU145
DUTXR
Downregulates genes
MAT2A (44kDa)
HIFα (93kDa)
MMP9 (92kDa)
MMP1 (54kDa)
Actin-β (54kDa)

Figure 4.

C.

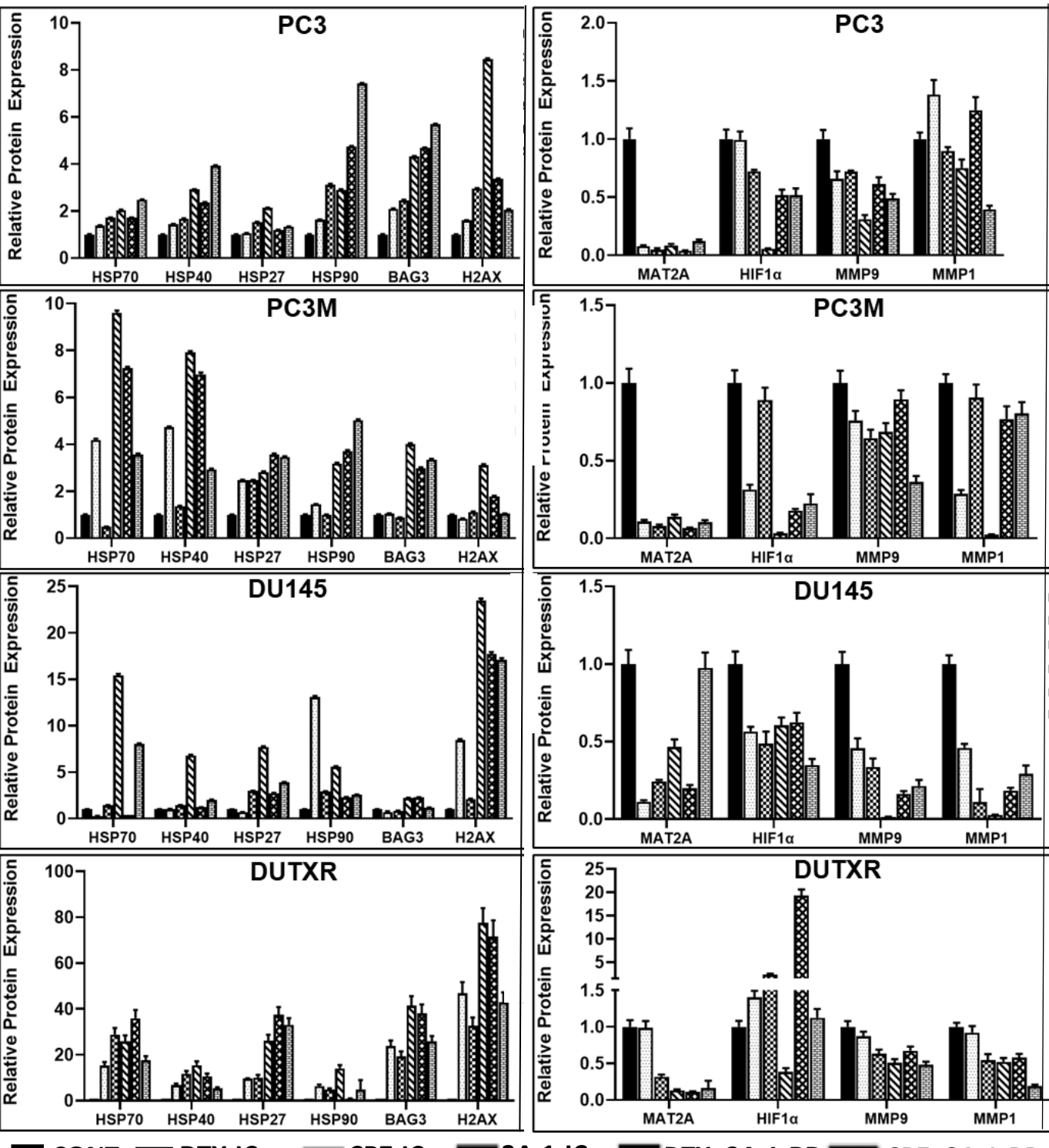
PC3
Relative Protein Expression
HSP70
HSP40
HSP27
HSP90
BAG3
H2AX
MAT2A
HIF1α
MMP9
MMP1
PC3M
DU145
DUTXR
CONT
DTX-IC50
CBZ-IC50
3A.1-IC50
DTX+3A.1-RD
CBZ+3A.1-RD

Figure 5.

A.

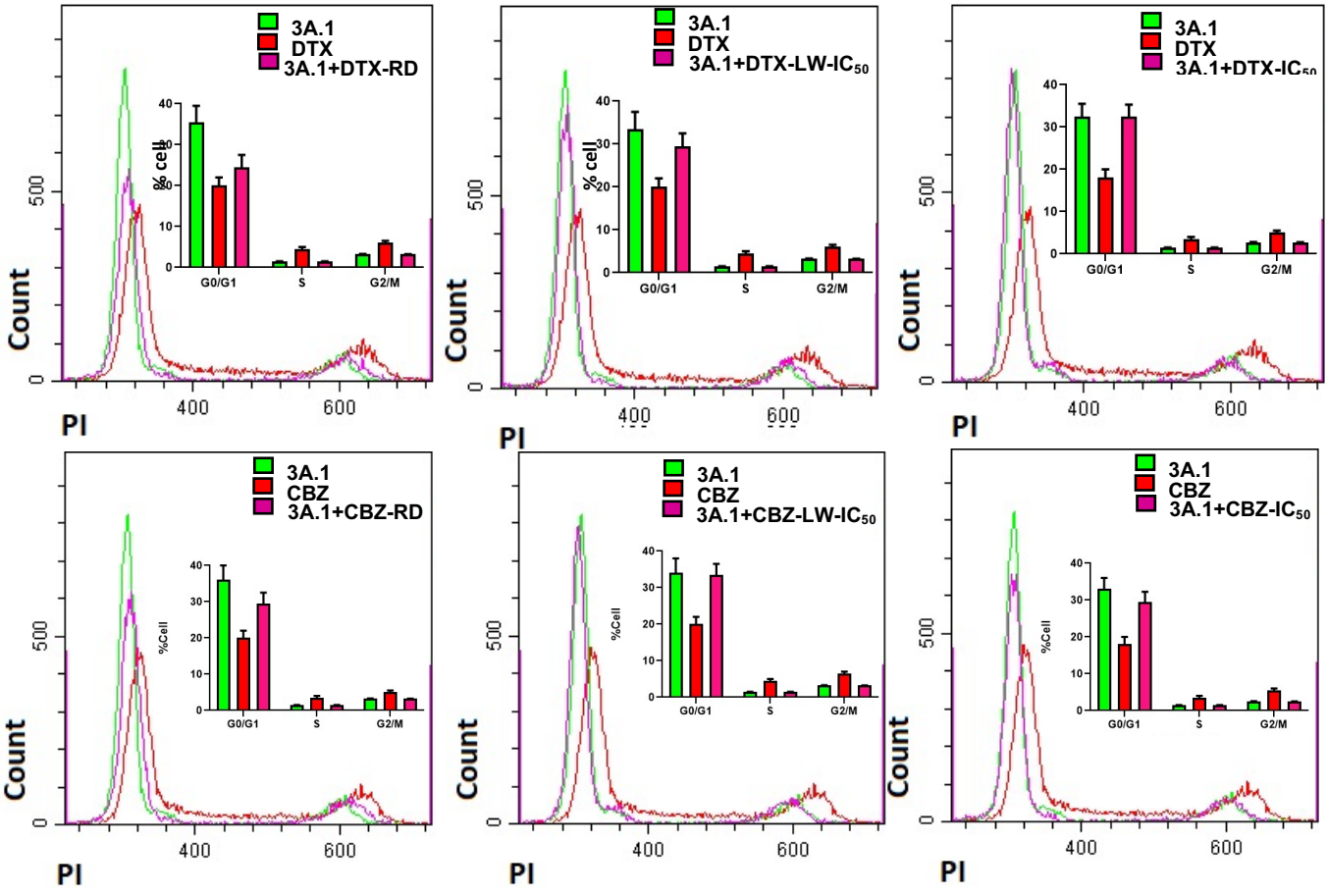
3A.1
DTX
3A.1+DTX-RD
3A.1+DTX-LW-IC50
3A.1+DTX-IC50
3A.1
CBZ
3A.1+CBZ-RD
3A.1+CBZ-LW-IC50
3A.1+CBZ-IC50
% cell
%Cell
G0/G1
S
G2/M
Count
PI
0
500
400
600
10
20
30
40

Figure 5.

B.

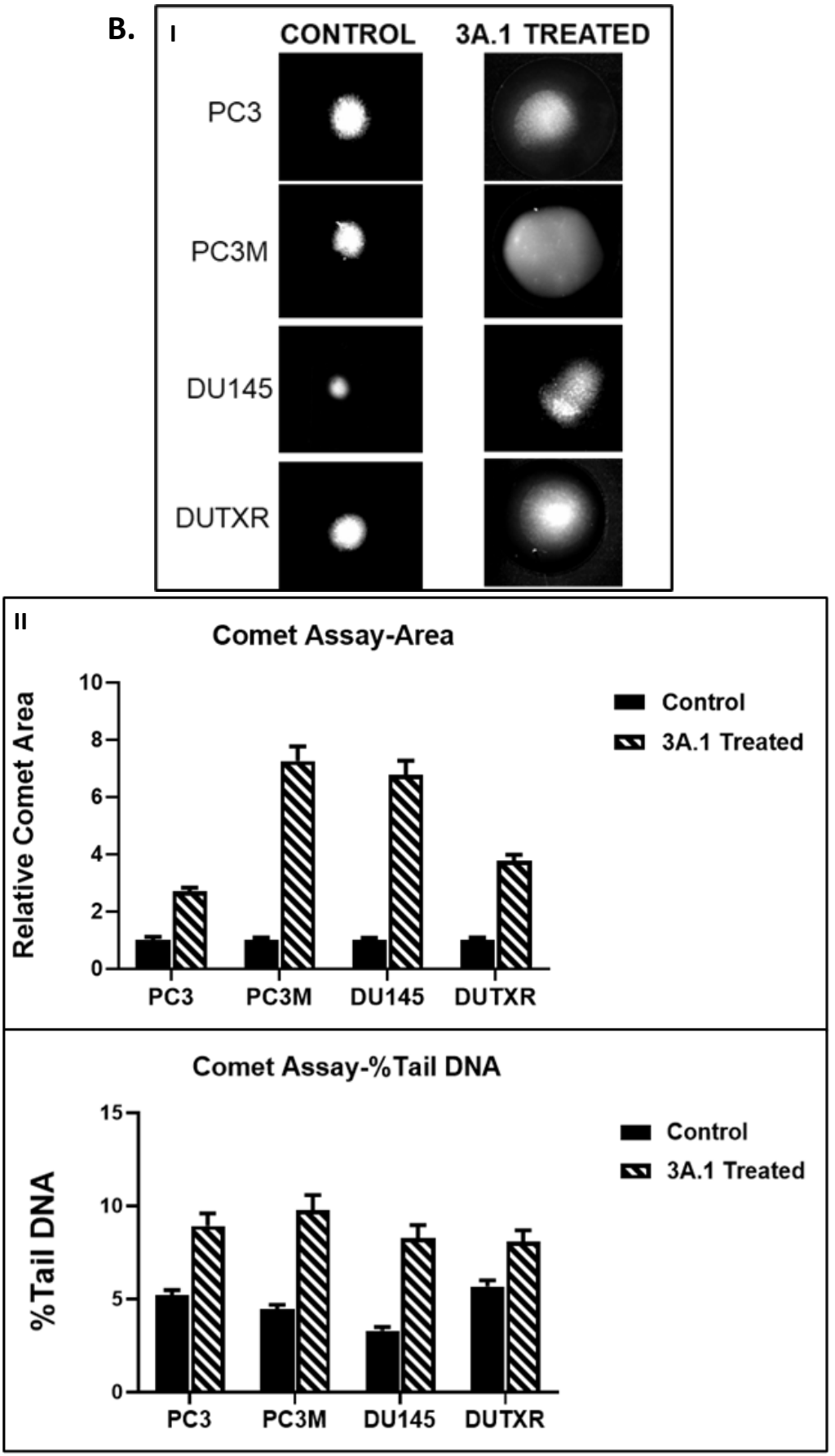
I
CONTROL
3A.1 TREATED
PC3
PC3M
DU145
DUTXR
II
Comet Assay-Area
Relative Comet Area
10
8
6
4
2
0
PC3
PC3M
DU145
DUTXR
Control
3A.1 Treated
Comet Assay-%Tail DNA
%Tail DNA
15
10
5
0
PC3
PC3M
DU145
DUTXR
Control
3A.1 Treated

Figure 5.

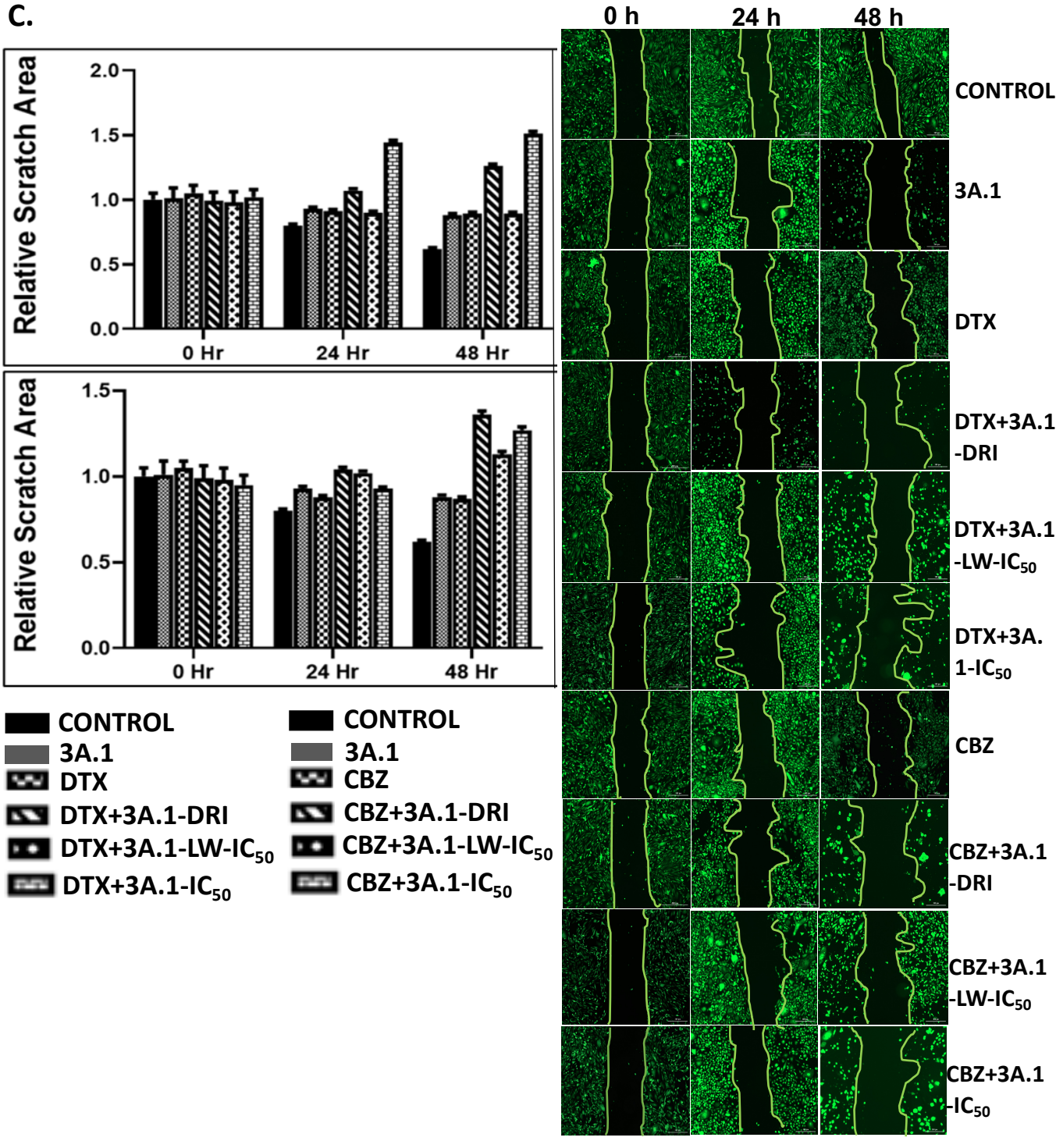
C.
0 h
24 h
48 h
Relative Scratch Area
2.0
1.5
1.0
0.5
0.0
0 Hr
24 Hr
48 Hr
Relative Scratch Area
1.5
1.0
0.5
0.0
0 Hr
24 Hr
48 Hr
CONTROL
3A.1
DTX
DTX+3A.1-DRI
DTX+3A.1-LW-IC50
DTX+3A.1-IC50
CONTROL
3A.1
CBZ
CBZ+3A.1-DRI
CBZ+3A.1-LW-IC50
CBZ+3A.1-IC50
CONTROL
3A.1
DTX
DTX+3A.1 -DRI
DTX+3A.1 -LW-IC50
DTX+3A. 1-IC50
CBZ
CBZ+3A.1 -DRI
CBZ+3A.1 -LW-IC50
CBZ+3A.1 -IC50